DRYING MECHANISM

OF HYGROSCOPIC POROUS BODY

HIRONOBU IMAKOMA

1984

DRYING MECHANISM
OF HYGROSCOPIC POROUS BODY

HIRONOBU IMAKOMA

1984

ACKNOWLEDGMENTS

The author would like to express his sincere appreciation to Professor Ryozo Toei of Department of Chemical Engineering Kyoto University for his valuable suggestions and encouragement throughout this work. He is also grateful to Associate Professor Morio Okazaki of Kyoto University for his helpful suggestions and valuable discussions.

The author wishes to express his sincere gratitude to Dr. Hajime Tamon of Kyoto Univesity, Associate Professor Masashi Asaeda of Hiroshima University, and Professor Takeshi Furuta of Toa University for their valuable suggestions.

Thanks are also due to Dr. Hiroyuki Kage, Dr. Takeshi Yamasaki and Dr. Takao Ohmori for their advices.

The author is grateful to Messrs. Masami Ono, Toshihiro Noda, Masaru Aimi, Kohsyun Ura, Kazuhito Goto and Noritake Satake for their assistances in the experimental or simulation works.

Acknowledgments are made to all the members of Laboratory of Professor Ryozo Toei, Kumiko Yoshinari and Kuniko Yamanaka for their helps in the preparation of this work.

Some parts of this work were supported by a Grant-in-Aid for Scientific research from the Ministry of Education, Science, and Culture.

The author tenders his gratitude to Sumitomo Aluminium Smelting Co., Ltd. for the supply of activated alumina.

The author is grateful to his parents for their encouragements and economical supports, and to Toyo Engineering Corp. for the financial assistance.

Finally, the author would like to express my gratitude to my partner, Ikuyo, for the moral support she has provided.

Hironobu Imakoma

Kyoto, December 1984.

CONTENTS

LIST OF SYMBOLS

A_d, A_m, A_p	surface area of sample, m^2
a	parameter defined by Eq. (2-33), dimensionless
B_0	viscous gas flow parameter, m^2
c	B.E.T. constant, dimensionless
D	transfer coefficient based on moisture content gradient, $m^2 \cdot s^{-1}$
D_K	Knudsen diffusivity, $m^2 \cdot s^{-1}$
D_{l0}	parameter defined by Eq. (2-32), dimensionless
D_{s0}	parameter defined by Eq. (2-33), dimensionless
D_{va}	binary diffusivity, $m^2 \cdot s^{-1}$
E_{a0}	differential heat of desorption, $J \cdot mol^{-1}$
E_{a1}	heat of evaporation, $J \cdot mol^{-1}$
E_{s1}	activation energy for migration in all layers above first layer, $J \cdot mol^{-1}$
h	thickness of adsorbed layer, m
J	mass transfer flux, $kg \cdot s^{-1} \cdot m^{-2}$
j	mol flux, $mol \cdot s^{-1} \cdot m^{-2}$
K_c	Kozeny constant (variable), dimensionless
K_{c0}	constant, dimensionless
$\overline{K}$	permeability, $m^2 \cdot s^{-1}$
k_g	film mass transfer coefficient, $kg \cdot Pa^{-1} \cdot s^{-1} \cdot m^{-2}$
L, L_d, L_m, L_p	length of sample, m
M	molecular weight, $kg \cdot mol^{-1}$

p	pressure, Pa
q	tortuosity factor, dimensionless
R	gas constant, $m^3 \cdot Pa \cdot K^{-1} \cdot mol^{-1}$
r	pore radius, m
S	specific surface area, $m^2 \cdot kg^{-1}$
s_d	surface area of glass tube, m^2
T	temperature, K
t	time, s
V	specific pore volume, $m^3 \cdot kg^{-1}$
u	velocity of oil piston, $m \cdot s^{-1}$
v	volume of glass bulb, m^3
X	moisture content, kg-H_2O·(kg-dry material)$^{-1}$
X_m	monolayer adsorbed amount of the B.E.T. equation, kg-H_2O·(kg-dry material)$^{-1}$
x	relative vapor pressure, dimensionless
Y	mol fraction, dimensionless
y	cartesian coordinate perpendicular to body surface,
z	$= (y/L)$, dimensionless
δ	length of dry zone, m
ε	porosity, dimensionless
μ	viscosity, Pa·s
θ	surface coverage according to the B.E.T. equation, dimensionless
ρ	density, $kg \cdot m^{-3}$

σ	surface tension, $N \cdot m^{-1}$

<Subscripts>

a	air
B	the B.E.T. equation
c	capillary (or critical in CHAPTER 7)
e	effective value
f	frictional value
l	liquid state water
mix	mixture or vapor and air
s	adsorbed water
$sapp$	apparent value of boby
t	total moisture including vapor
v	vapor
0	standard

<Superscripts>

d	diffusion
v	viscous gas flow
*	saturation
$-$	average

CHAPTER 1 INTRODUCTION

1.1 Purpose and Scope of This Thesis

The drying of porous materials is one of the most important unit operations in chemical engineering. In order to design drying processes it is desirable to have a mathematical model capable of describing the drying process quantitatively.

The mathematical model is also applied to other requirements. For example during the preparation of supported catalysis, it is necessary to know the redistribution of solute as the solvent is removed by drying [13]. The drying of soils in a land treatment system is offered as another example, related to disposing municipal and certain industrial waste waters on land [14]. If the concept of drying is expanded into the isothermal system as an special case, the mathematical model can be applied to fields of the soil physics and the petroleum technology etc.

At present, two drying models are generally accepted, one is Krischer's model [10], and the other is Luikov's approach [11]. Krischer considered that the moisture transfer in porous bodies is controlled by some combination of capillary

water flow and vapor diffusion. In order to express the capillary water flow rate during drying, he introduced what is called the parallel pore model. Toei [19][21] modified the model using the Kozeny-Carman equation on the basis of the similar physical idea of a combination of water flow and vapor transfer to Krischer's one. Krischer's physical idea has been developed into that on a non-isothermal system [2] [14]. Luikov, on the other hand, intended the thermodynamics of irreversible processes to apply the transport phenomena on drying and his school has achieved distinctions in this field [6].

In order to present a mathematical model, it is noted that there are two key points. The first one is that transport properties within porous bodies, namely effective water-vapor diffusivities, the liquid water transfer coefficient and so on, should be determined entirely independent of any drying experiments. The second point is that unknown parameters introduced in the mathematical expressions of the transport properties have to be dependent only on structure characteristics of porous bodies, in other words these parameters have to be completely independent of the internal potentials, for example temperature, moisture content , or partial vapor and total pressures. Despite of the fact that many efforts have been made in the past to

develop mathematical models, almost all models seem to be unsatisfactory from the viewpoints above mentioned.

The moisture transfer including the water-vapor transfer within rigid porous bodies on drying processes has already been analysed qualitatively [22]. It is difficult to express the transport properties in transport equations with the physical parameters depending only on pore structure characteristics, because moisture may exists within porous bodies in liquid or vapor form and phase interchanges may occur during drying processes. In addition, the most important difficulty lies in the fact that moisture may be transferred by several different mechanisms within bodies. Especially, the surface flow phenomenon on the solid surface has not sufficiently been analysed yet, and the transfer due to a temperature gradient has been almost unknown.

The drying is the simultaneous heat- and mass- transport phenomena, and so it is necessary to solve the simultaneous transport equations owing to clarify the mechanism of drying. Since the mass transport phenomena within the hygroscopic porous body is so complicated and especially the surface flow due to a temperature gradient is almost unknown as is mentioned above, in this thesis, mathematical expressions are derived under an isothermal condition. This

treatment can be acceptable from a phenomenological point of view that parts of practical drying processes are regarded as isothermal systems, and it is noted that

(1) these expressions include parameters depending only on the pore structure characteristics and

(2) the parameters have to be determined entirely independent of any drying experiments.

Futhermore, the other purpose on this work is to develop a general drying (mass-transfer) model applicable to both hygroscopic and non-hygroscopic porous bodies.

In CHAPTER 2, a drying model for hygroscopic microcapillary-porous body is introduced and then mathematical expressions for the transport of water-vapor, capillary condensed water, and adsorbed water within porous bodies on the drying process under isothermal condition are derived.

CHAPTER's 3 and 4 deal with measurement of transport properties which are introduced into transport equations in CHAPTER 2, and CHAPTER 3 refers to widely used measurement techniques to determine pore structure characteristics and transport properties within porous bodies. In CHAPTER 4, a new measurement method of hygroscopic microcapillary porous bodies for (adsorbed and capillary condensed) water transfer

coefficient is described. This coefficient has never been obtained excepting by drying experiments till now.

In CHAPTER 5, a reliability of the water transfer coefficient obtained in CHAPTER 4 is confirmed through an isothermal vacuum drying experiment of a hygroscopic porous material, because the vacuum drying is the simplest case of the gaseous transpot phenomena.

CHAPTER 6 deals with a verification of all the proposed mathematical transport expressions with an isothermal convection drying experiment of a hygroscopic porous material.

In CHAPTER 7, The proposed mathematical model is applied to a non-hygroscopic macrocapillary porous material on an isothermal convection drying process as a more simple case, and it is certified that this model can also simulate well the isothermal drying process of the non-hygroscopic material.

In conclusion, the advantages and disadvantages of the proposed drying model are discussed in CHAPTER 8, and from the discussions the problems for the future work are pointed out.

1.2 Publications on This Thesis

CHAPTER's 2, 3, and 6:

ACTA POLYTECHNICA SCANDINAVICA, Chemical Technology and Metallurgy Series, to be published

CHAPTER 4: Journal of Chemical Engineering of Japan, vol.16, 5, pp 364 - 369 (1983).

CHAPTER's 4 and 5:

Proceedings of the Third International Drying Symposium, vol.1, pp 65 - 76 (1982).

CHAPTER 5: Journal of Chemical Engineering of Japan, vol.16, 5, pp 431 - 432 (1983).

CHAPTER 7: Journal of Chemical Engineering of Japan, vol.18, 2 (1985).

CHAPTER 2 BASIC THEORY

2.1 Drying Model for Hygroscopic Microcapillary-porous Body

A proposed model for the drying of hygroscopic (adsorptive) porous body with microcapillaries underlying the mathematical expressions can be described as follows. However, the model is developed under an isothermal condition, because it has not been understood sufficiently about the surface flow phenomenon due to a gradient in temperature.

The water (moisture) held in the hygroscopic porous body is classified into three groups; the adsorbed water on the solid surface, the condensed water in microcapillaries, and the water vapor within the gas void. In this thesis, the void within the porous body is idealized as a bundle of circular microcapillaries which have a distribution of radius. The amount of water adsorbed on capillary walls is estimated by the B.E.T. equation, and that of capillary condensed water is estimated in accordance with the Kelvin equation. The water-vapor pressure within the gas void and the moisture content, which is the sum of amount of adsorbed and capillary condensed water, are in equilibrium at any location within the wet porous body, if the rate of phase

change is much faster than that of mass transfer. In other words, the vapor pressure can be governed by the adsorption or desorption isotherm.

The adsorbed water is transferred by surface flow due to a gradient in adsorbed amount, the condensed water by capillary flow due to a gradient in capillary pressure, and the water vapor by gaseous diffusion due to a gradient in partial vapor pressure. The total pressure within the wet porous body, however, becomes larger than the atmospheric one even under ordinary drying conditions in case of coexisting air. We have to consider the effect of this generated pressure on the transfer rate of the condensed water and water vapor.

The "dusty-gas model" [12] is applied to transport of the water vapor within a porous body. Though the two components, water vapor and air, exist in the gas void within the drying body, since the drying process is approximated as a unidirectional diffusion process, the air flux can be ignored. This assumption means that the influx of air due to a partial air-pressure gradient is canceled with its outflow due to the generated total-pressure gradient, from a physical viewpoint.

Secondly, the "modified Kozeny-Carman model" [19][21] is applied to movement of the capillary condensed water. The "modified Kozeny-Carman model" is some combination of the Kozeny-Carman model and the parallel pore model [10]. The drying process of porous bodies can be regarded as that of dehydration from the larger capillaries in accordance with the parallel pore model. Though the Kozeny-Carman equation can be applied to the flow in a porous body when the void is filled with one fluid (gas or liquid), this equation is applied to the wet part of an unsaturated wet porous body on the "modified Kozeny-Carman model". The specific surface area and the porosity in the Kozeny-Carman equation, therefore, change with moisture content on the "modified Kozeny-Carman model".

The transfer coefficient of condensed water within an activated alumina, which is an example for the hygroscopic microcapillary-porous body, obtained experimentally in CHAPTER 4 is tried to explain with the "modified Kozeny-Carman model", and the Kozeny constant is not a constant but a variable, that varies inversly to the ratio of the amount of capillary condensed water to the total moisture content as a result. In this thesis, therefore, the relation of the Kozeny constant with the condensed water content is introduced in the proposed model as an assumption.

Finally the "modified hopping model" [16] is applied to migration of the water molecules adsorbed on the capillary walls. As the surface area within the drying body is increased with drying, the value of surface area can be determined using the parallel pore model similar to the case of the condensed water flow.

In this thesis, the total flux of water within the drying body is written as a sum of the flux of water vapor, capillary condensed water, and adsorbed water; $J_t = J_v + J_l + J_s$, assuming that there are no interactions one another. In order to determine moisture-content profiles within porous bodies during drying, it is convenient that these transport properties are transformed into properties whose driving forces are defined by a gradient in moisture content. The total flux of water is given, therefore, by the product of a coefficient and the moisture-content gradient.

$$J_t = - \rho_{sapp} D_t \frac{dX}{dy} \qquad (2\text{-}1)$$

where

$$D_t = D_v + D_l + D_s$$

2.2 Prediction of Desorption Isotherm

The liquid water held in hygroscopic (adsorptive) porous bodies is classified into the adsorbed water on the wall of capillaries, X_s, and the condensed water in the capillaries, X_l. It is considered that there exsists the radius distribution of micro-capillary in the body between r_{min} and r_{max}, and the adsorbed amount of water can be given by the B.E.T. equation.

When the value of vapor pressure is p_{v0}, an uniform adsorbed layer of thickness $h_0 = (\rho_l X_B / S_t)$ is formed on the wall of all capillaries. All of the capillaries of radius $r \leqq r_0 + h_0$ are filled with the condensed water, where r_0 is called the Kelvin radii and determined from the following Kelvin equation.

$$\ln(p_v^*/p_{v0}) = (2\sigma_l M_v)/(r_0 R T \rho_l) \qquad (2\text{-}2)$$

Consequently, all the liquid water held in the capillaries of radius $r \leqq r_0 + h_0$ is the condensed water, and the water adsorbed on the wall of the capillaries of radius $r > r_0 + h_0$ is the adsorbed water.

The following four variables can be calculated using the

cumulative pore-volume, $V(r)$, and surface-area, $S(r)$, distribution functions (cf. Fig 3-1).

$$X_s = X_B \frac{S(r_0 + h_0)}{S_t} \quad , \qquad S_s = S(r_0 + h_0) \tag{2-3}$$

$$X_l = \rho_l [V_t - V(r_0 + h_0)] \quad , \qquad S_l = S_t - S_s \tag{2-4}$$

where X_B is the adsorbed amount of water determined by the B.E.T. equation, and expressed as follows.

$$X_B = \frac{X_m \, c \, (p_{v0}/p_v^*)}{[1 - (p_{v0}/p_v^*)][1 - (p_{v0}/p_v^*) + c(p_{v0}/p_v^*)]} \tag{2-5}$$

where X_m means the maximum monolayer adsorbed amount. The isotherm for the capillary condensation region, therefore, can be predicted using $V(r)$, $S(r)$, and the adsorption data, capable of determining the parameters, X_m and c, in the B.E.T. equation. The moisture content, X, can be determined by the sum of contents of adsorbed water, X_s , and the capillary condensed water, X_l.

2.3 Vapor Diffusion and Flow

Mason et al. [12] proposed an idea, based on the dusty gas model, that the flux of i-th component can be given by

$$j_i = j_i^d + Y_i j^f \tag{2-6}$$

where j_i^d is the molar flux at isobaric diffusion, Y_i is the mol fraction of the i-th component and j^f is the total viscous flow flux. As the component i represents water vapor or air as is mentioned above, the flux of vapor or air is defined by

$$j_v = j_v^d + Y_v j^f \tag{2-7}$$

$$j_a = j_a^d + Y_a j^f \tag{2-8}$$

The diffusional flux of vapor or air at uniform-pressure becomes

$$\frac{1}{D_{vae}}(Y_a j_v^d - Y_v j_a^d) + \frac{1}{D_{Kve}} j_v^d = -\frac{1}{RT}\frac{dp}{dy}v \tag{2-9}$$

$$\frac{1}{D_{vae}}(Y_v j_a^d - Y_a j_v^d) + \frac{1}{D_{Kae}} j_a^d = -\frac{1}{RT}\frac{dp}{dy}a \tag{2-10}$$

The sum of Eqs. (2-9) and (2-10) becomes

$$\frac{1}{D_{Kve}} j_v^d + \frac{1}{D_{Kae}} j_a^d = - \frac{1}{RT}\left(\frac{dp}{dy}_v + \frac{dp}{dy}_a\right) \qquad (2\text{-}11)$$

Futhermore, the total flux of viscous flow is written as

$$j^f = - \frac{B_0 p_t}{\mu_{mix} RT} \frac{dp_t}{dy} \qquad (2\text{-}12)$$

If one ignores the flux of air as is mentioned in Section 2.1; $j_a = 0$, the flux of water vapor is obtained as Eq. (2-13) from substituting Eqs. (2-7), (2-8) and (2-12) into Eq. (2-11)

$$j_v = \frac{D_{Kve}}{RT}\left[1 + \left(\frac{p_v}{D_{Kve}} + \frac{p_t - p_v}{D_{Kae}}\right)\frac{B_0}{\mu_{mix}}\right]\frac{dp}{dy}t$$

$$= Q \frac{dp}{dy}t \qquad (2\text{-}13)$$

Besides the relationship between p_t and p_v can be introduced as follows:

Equations (2-9) and (2-10) are transformed as

$$j_v^d = - \frac{D_{ve}}{RT} \frac{dp}{dy}_v + Y_v \frac{D_{ve}}{D_{vae}} j_t^d \qquad (2\text{-}14)$$

$$j_a^d = - \frac{D_{ae}}{RT} \frac{dp}{dy}_a + Y_a \frac{D_{ae}}{D_{vae}} j_t^d \qquad (2\text{-}15)$$

where

$$(1/D_{ie}) = (1/D_{Kie}) + (1/D_{vae})$$

The sum of these eqution is given by

$$j_t^d = - \frac{1}{RT} \frac{D_{ve}\frac{dp_v}{dy} + D_{ae}\frac{dp_a}{dy}}{1 - \frac{D_{ve}}{D_{vae}}Y_v - \frac{D_{ae}}{D_{vae}}Y_a} \qquad (2\text{-}16)$$

By substituting Eq. (2-16), Eq. (2-15) becomes

$$j_a^d = - \frac{D_{ae}}{RT}\frac{dp_a}{dy} - \frac{Y_a}{RT}\frac{D_{ae}}{D_{vae}} \frac{D_{ve}\frac{dp_v}{dy} + D_{ae}\frac{dp_a}{dy}}{1 - \frac{D_{ve}}{D_{vae}}Y_v - \frac{D_{ae}}{D_{vae}}Y_a} \qquad (2\text{-}17)$$

The total flux of air is assumed to be ignored as is mentioned above,

$$j_a^d = - Y_a \, j^f \qquad (2\text{-}18)$$

and consequently the relationship between p_t and p_v is written as Eq. (2-19) by substituting Eqs. (2-12) and (2-17) into Eq. (2-18).

$$\frac{dp_t}{dp_v} = \frac{D_{ae} - \frac{D_{ae}(D_{ve} - D_{ae})(p_t - p_v)}{(D_{vae} - D_{ae})p_t + (D_{ae} - D_{ve})p_v}}{D_{ae} + \frac{(D_{ae})^2(p_t - p_v)}{(D_{vae} - D_{ae})p_t + (D_{ae} - D_{ve})p_v} + \frac{B_0}{\mu_{mix}}(p_t - p_v)} \qquad (2\text{-}19)$$

Combining Eqs. (2-13) and (2-19), j_v can be given by

$$j_v = - Q \frac{dp_t}{dp_v}\frac{dp_v}{dy} \qquad (2\text{-}20)$$

The mass flux, therefore, is written as

$$J_v = - \rho_{sapp} \frac{M_v}{\rho_{sapp}} Q \left(1 - \frac{X}{X^*}\right) \frac{dp_t}{dp_v} \frac{dp_v}{dX} \frac{dX}{dy}$$

$$= - \rho_{sapp} D_v \frac{dX}{dy} \qquad (2\text{-}21)$$

where the term $(1 - X/X^*)$ is the ratio of the volume of vacant pores to the total void volume within the body and dp_v/dX is calculated using the desorption isotherm, namely through Eqs. (2-2) - (2-5).

It is useful to know the following two special cases.

(1) Single-component (vapor) flow

Let $p_t = p_v$, Eq. (2-21) is written as

$$J_v = - \rho_{sapp} \frac{M_v}{RT\rho_{sapp}} \left(D_{Kve} + \frac{B_0}{\mu_v} p_v\right)\left(1 - \frac{X}{X^*}\right) \frac{dp_v}{dX} \frac{dX}{dy} \qquad (2\text{-}22)$$

(2) Uniform-pressure diffusion

In this case, it is not adequate to apply Eq. (2-21), because this equation is derived through the assumption of Eq. (2-18), namely the total flux of air is zero. Accordingly another simple transformation is required as follows:

As the total pressure gradient is zero in case of uniform-pressure diffusion, Eq. (2-11) becomes

$$j_a^d = - \frac{D_{Kae}}{D_{Kve}} j_v^d \qquad (2\text{-}23)$$

From substituting this equation into Eq. (2-9), the following one is obtained.

$$j_v = - \frac{D_{Kve}}{RT} \frac{D_{vae}}{D_{vae} + [(p_t - p_v)/p_t]D_{Kve} + (p_v/p_t)D_{Kae}} \frac{dp_v}{dy} \quad (2\text{-}24)$$

2.4 Viscous Flow of Capillary Condensed Water

When the liquid water flow in a fine capillary to the drying surface during drying, the force balance among capillary pressure, total pressure, and frictional force over an infinitely small distance dy yields Eq. (2-25) neglecting the effect of gravitational force.

$$(\frac{dp_c}{dy})dy - (\frac{dp_t}{dy})dy = (\frac{dp_f}{dy})dy \quad (2\text{-}25)$$

When the condensed water within a porous body flows in accordance with the Kozeny-Carman equation based on the "modified Kozeny-Carman model" [19][21], a flux is given by

$$J_l = \frac{\rho_l[\rho_{sapp}(X_l/\rho_l)]^3}{\mu_l K_c(\rho_{sapp}S_l)^2} \frac{dp_f}{dy} = \psi\frac{dp_f}{dy} = \psi(\frac{dp_c}{dy} - \frac{dp_t}{dy}) \quad (2\text{-}26)$$

The differential form of the Kelvin equation is introduced to convert a capillary pressure gradient into a vapor pressure one.

$$\frac{dp_c}{dy} = - \frac{\rho_l RT}{M_v p_v} \frac{dp_v}{dy} \qquad (2\text{-}27)$$

where the relation between the capillary pressure, p_c, and the capillary radius, r, is used to eliminate r in the Kelvin equation.

$$p_c = 2\sigma_l / r \qquad (2\text{-}28)$$

From Eqs. (2-26) and (2-27), the flux of capillary condensed water can be written as

$$\begin{aligned} J_l &= - \psi \frac{\rho_l RT}{M_v p_v} \frac{dp_v}{dy} - \psi \frac{dp_t}{dy} \\ &= - \psi \left(\frac{\rho_l RT}{M_v p_v} \frac{dp_v}{dp_t} + 1 \right) \frac{dp_t}{dy} \end{aligned} \qquad (2\text{-}29)$$

The first term in the parentheses is a contribution of capillary pressure and the second one is that of total pressure.

For instance at 100°C

$$\frac{\rho_l RT}{M_v p_v} \frac{dp_v}{dp_t} \geq \frac{\rho_l RT}{M_v p_v^*} \cong 1600 >> 1$$

It is reasonable to consider only the capillary condensed water flow due to a gradient in capillary pressure.

Consequently the flux of condensed water can be approximated as follows.

$$J_l = -\psi \frac{\rho_l RT}{M_v p_v} \frac{dp_v}{dy} = -\frac{RT\rho_{sapp}}{\rho_l \mu_l K_c M_v p_v} \frac{X_l^3}{S_l^2} \frac{dp_v}{dy}$$

$$= -\rho_{sapp} \frac{RT_0 (X^*)^3}{\rho_l K_c M_v S_t^2 \mu_{l0}} \left(\frac{T}{T_0}\right) \left(\frac{\mu_{l0}}{\mu_l}\right) \left(\frac{X_l}{X^*}\right)^3 \left(\frac{S_t}{S_l}\right)^2 \left(\frac{1}{p_v}\right) \frac{dp_v}{dX} \frac{dX}{dy}$$

$$= -\rho_{sapp} D'_{l0} \left(\frac{T}{T_0}\right) \left(\frac{\mu_{l0}}{\mu_l}\right) \left(\frac{X_l}{X^*}\right)^3 \left(\frac{S_t}{S_l}\right)^2 \left(\frac{1}{p_v}\right) \frac{dp_v}{dX} \frac{dX}{dy} \qquad (2\text{-}30)$$

The Kozeny constant in Eq. (2-30) is assumed as a function of the moisture content as is mentioned in Section 2.1, and the following expression is obtained from the correlation of Eq. (2-30) with the experimental data in CHAPTER 4. The correlation method will be described in Section 4.3.

$$K_c = K_{c0} (X^*/X_l) \qquad (2\text{-}31)$$

Finally, Eq. (2-30) becomes

$$J_l = -\rho_{sapp} \frac{RT_0 (X^*)^3}{\rho_l K_{c0} M_v S_t^2 \mu_{l0}} \left(\frac{T}{T_0}\right) \left(\frac{\mu_{l0}}{\mu_l}\right) \left(\frac{X_l}{X^*}\right)^4 \left(\frac{S_t}{S_l}\right)^2 \left(\frac{1}{p_v}\right) \frac{dp_v}{dX} \frac{dX}{dy}$$

$$= -\rho_{sapp} D_{l0} \left(\frac{T}{T_0}\right) \left(\frac{\mu_{l0}}{\mu_l}\right) \left(\frac{X_l}{X^*}\right)^4 \left(\frac{S_t}{S_l}\right)^2 \left(\frac{1}{p_v}\right) \frac{dp_v}{dX} \frac{dX}{dy}$$

$$= -\rho_{sapp} D_l \frac{dX}{dy} \qquad (2\text{-}32)$$

2.5 Surface Flow of Adsorbed Water Molecules

The water molecules are adsorbed on the pore wall within the hygroscopic micro-capillary porous body and the adsorbed molecules migrate on the surface. If the adsorbed amount can be given by the B.E.T. equation, the flux of surface flow can be written as Eq. (2-33) based on the "modified hopping model" [15]. The term S_s/S_t of Eq. (2-33) represents the decrease of surface area, where the surface flow occurs, due to the capillary condensation, according as vapor pressure p_v increases.

$$J_s = -\rho_{sapp} D_{s0} \frac{(1 \quad x)[\exp(-aE_{a0}/RT) - \exp(-E_{a0}/RT)]}{[1 - \exp(-E_{a0}/RT)]\{1 - \theta(1 - x)[1 - (\tau_1/\tau_0)]\}} \times (S_s/S_t) \frac{dX_B}{dX} \frac{dX}{dy} = - \rho_{sapp} D_s \frac{dX}{dy} \qquad (2\text{-}33)$$

where

$$\tau_1/\tau_0 = \frac{[1 - \exp(-E_{a1}/RT)][\exp(-aE_{a0}/RT) - \exp(-E_{a0}/RT)]}{[1 - \exp(-E_{a0}/RT)][\exp(-E_{s1}/RT) - \exp(-E_{a1}/RT)]}$$

This mathematical form is derived in the case of the solid surface possessing a energetical homogeneous one.

CHAPTER 3 PHYSICAL CHARACTERISTICS AND VAPOR TRANSPORT PROPERTIES IN HYGROSCOPIC CAPILLARY-POROUS BODY

3.1 Cumulative Pore-volume and Surface-area Distributions

Among the various methods of pore structure investigation, the mercury penetration and the nitrogen sorption-condensation (at -196 ℃) techniques have achieved popularity for measuring pore-size distributions. In this thesis, these techniques are used to determine the pore-size distributions. It is well known that the mercury penetration technique consists of measuring simultaneously the capillary pressure and the volume of mercury that has penetrated the sample up to that pressure. This gives the cumulative pore-volume distribution from which the internal surface-area distribution can be obtained using the cylindrical pore model. This technique is useful to determine the pore characteristics in the range of pore radii down to 1.5nm. Though it is evident that this technique does not detect the dimensions of the pores into that the mercury can be intruded only through necks narrower than the pore itself, this technique is useful as drying processes are always regarded as desorption ones.

Another technique of pore structure investigation applied in

this thesis is the nitrogen sorption-condensation (at -196 ℃) one. There are various computational methods to calculate pore-size distributions from desorption isotherms by using the cylindrical pore model, and the method of Dollimore and Heal [5] that is one of the most famous ones among them is adopted.

Three experimental materials are used as drying bodies in this thesis. Two of them are hygroscopic (adsorptive) microcapillary-porous materials, and one is an activated alumina and the other is also an activated alumina which has relatively coarse pores compared with the former one but has similar adsorption capacity. The cumulative pore-volume distributions of the both activated alumina are determined by combining the mercury penetration (solid lines) and the nitrogen sorption-condensation (broken lines) techniques as is shown in Fig. 3-1. The desorption isotherms of these samples were observed only up to pore radii about 7nm owing to the experimental difficulties. The mercury porosimeter used, on the other hand, covered a range of pore radii from 2nm up to 100μm. The pore-volume distribution determined by the mercury penetration technique in the range of pore radii from 2nm to 7nm fits the distribution from the desorption isotherm in each activated alumina, when the contact angle of mercury against the solid surface is 138°,

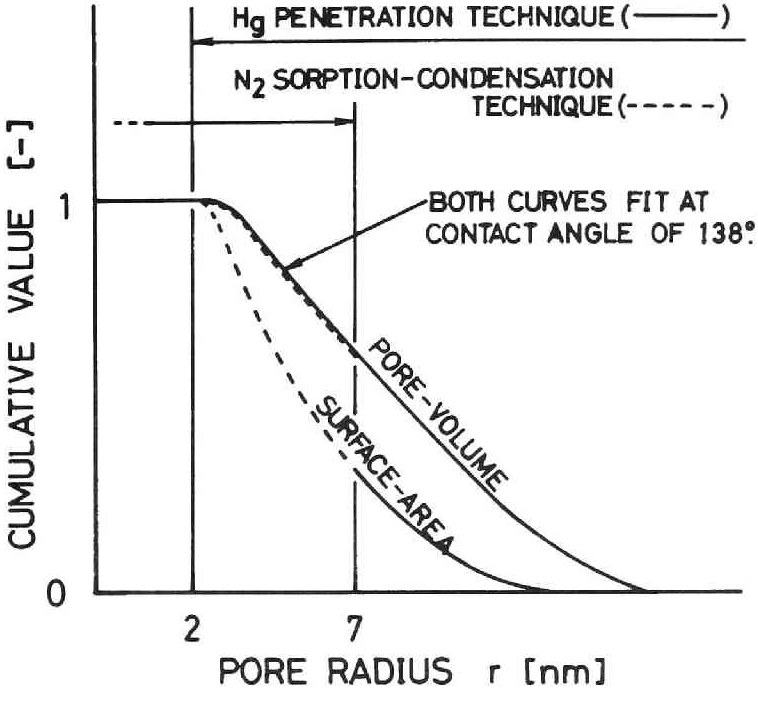

Fig. 3-1. Determination method of cumulative distributions for activated alumina.

that is a suitable value compared with the commonly used ones. On the other hand, the cumulative surface-area distributions by the mercury penetration technique and from the desorption isotherms are used as the experimental results in the range of pore radii above 7nm and from 2nm to 7nm, respectively.

The remainder one of the three materials is an unglazed alumina-based ceramic which is a non-hygroscopic capillary porous material. Cumulative distributions by the mercury penetration technique are used as experimental results.

3.2 Effective Knudsen Diffusivity and Viscous Gas Flow Parameter

Apparatus of the permeability measurements are classified into two types; quasi-stationary, that is constant volume methods and stationary methods. In this thesis, the constant volume method was employed to measure the permeabilities.

The schematic diagram of an apparatus for constant volume method [8] is shown in Fig. 3-2. An adhesive resin (Torr Seal) was applied to attach a disc of experimental material to the diverging glass pipes, and the apparatus is mounted in the temperature controlled box.

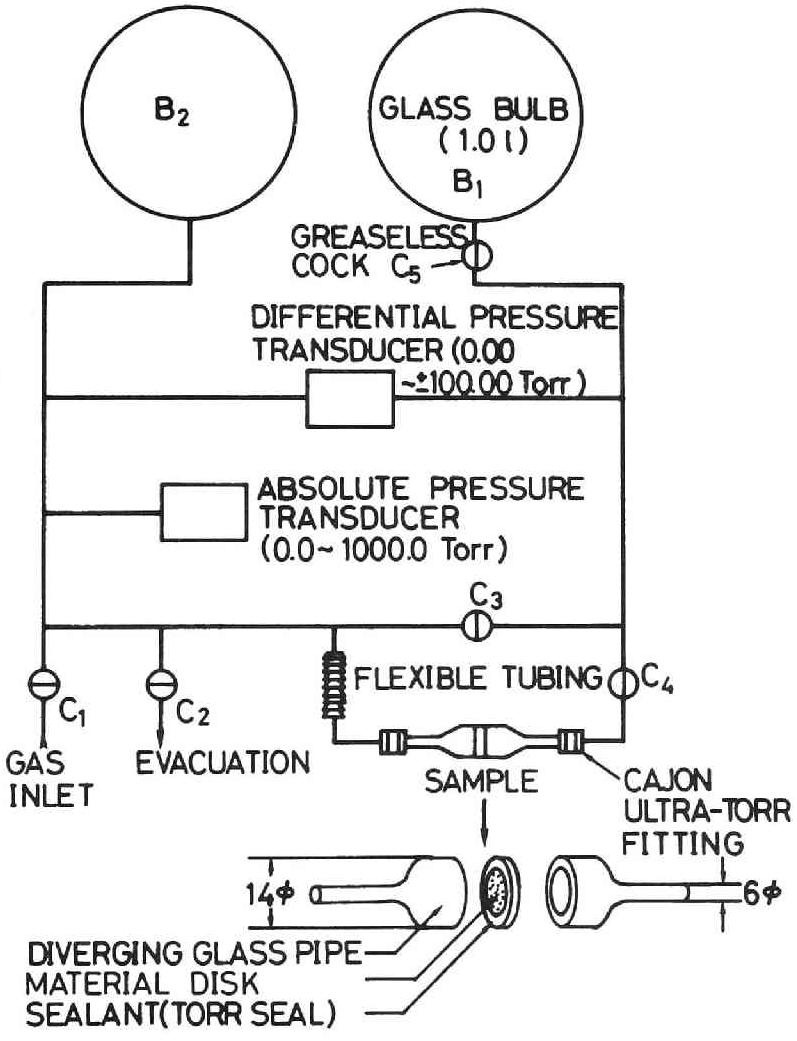

Fig. 3-2. Schematic diagram of permeation apparatus.

(constant volume method)

The principle of analysis for this method is as follows. Suppose two glass bulbs (B_1 and B_2) with known volumes, v_1 and v_2 ($v_1 \simeq v_2$), which are separated by a porous plug and there is a differential pressure between them ($p_1 < p_2$). When the accumulation of gas in the plug is negligible compared with the flux across it, the rate of accumulation of the gas in the glass bulb B_1 is equated with the rate of influx to it.

$$v_1 \frac{dp_1}{dt} = \frac{A_p}{L_p} K(p_1 - p_2)$$

$$= \frac{A_p}{L_p} K[p_1(1 + \frac{v_1}{v_2}) - \frac{p_{10}v_1 + p_{20}v_2}{v_2}] \qquad (3\text{-}1)$$

This equation is solved with the initial condition that

$$t = 0 ; \quad p_1 = p_{10} \qquad (3\text{-}2)$$

and yields

$$p_1 - \alpha = (p_{10} - \alpha)\exp(-\beta t) \qquad (3\text{-}3)$$

where

$$\alpha = \frac{p_{10}v_1 + p_{20}v_2}{v_1 + v_2} \quad \text{and} \quad \beta = \frac{A_p K}{L_p v_1}(1 + \frac{v_1}{v_2}) \qquad (3\text{-}4)$$

Taking logarithms of both sides of Eq. (3-3), one has

$$\log_{10}(p_1 - \alpha) = -(\beta/2.303)t + \log_{10}(p_{10} - \alpha) \qquad (3\text{-}5)$$

A plot of $\log_{10}(p_1 - \alpha)$ vs. t is expected to give a straight line with a slope of $-(\beta/2.303)$, intercepting at $(p_{10} - \alpha)$. Thus, from the slope and Eq. (3-4), a permeability of sample, K, can be determined.

The permeability, on the other hand, is written as Eq. (3-6), when a non-adsorbable gas A is used.

$$K = D_{Ke} + (B_0/\mu)p \qquad (3\text{-}6)$$

where

$$p = (p_{10} + p_{20})/2$$

The value of effective Knudsen diffusivity, D_{KAe}, and viscous gas flow parameter, B_0, can be calculated from a plot of K vs. p also using the above-mentioned procedure. An example of the plot is shown in Fig. 3-3.

Since the effective Knudsen diffusivities are independent of the pressure but dependent on the temperature and the molecular weight, consequently, the effective diffusivities of water-vapor and air are given by the following equations using the effective Knudsen diffusivity of the

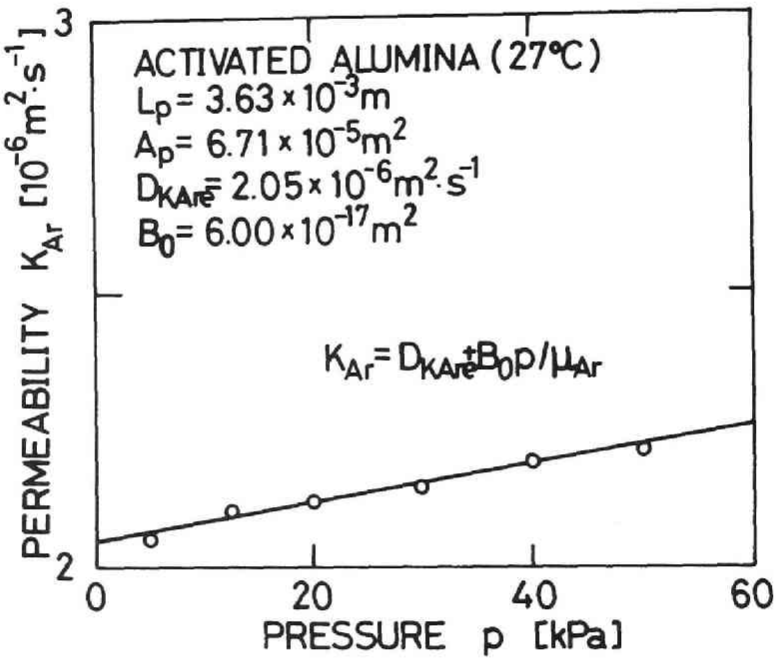

Fig. 3-3. An experimental result of permeation experiment. (using Ar-gas)

non-adsorbable gas A, D_{KAe}, at an arbitrary temperature.

$$D_{Kve} = D_{KAe}|_{T_0} \sqrt{M_A T/(M_v T_0)} \tag{3-7}$$

$$D_{Kae} = D_{KAe}|_{T_0} \sqrt{M_A T/(M_a T_0)} \tag{3-8}$$

3.3 Effective Binary Diffusivity

Usually the diffusion of gases through porous body is studied experimentally by an apparatus such as the Wicke-Kallenbach type. A different method [1], however,was employed in this thesis.

Consider a glass bulb to which a sealed sample and a small tube are attached as shown in Fig. 3-4. Non-adsorbable gases, A and B ($M_A < M_B$), are used, and Gas A in the glass bulb is sealed by a movable oil piston and Gas B is flowing along the outside path. The net flow rate, $j_A + j_B$, can be measured by observing the moving speed of the piston which moves so as to make the pressures on both sides of the sample equal.

When the influx amount of Gas B is sufficiently small in some time-interval in comparison with the amount of Gas A in the glass bulb, the flux equation of Gas A can be written as

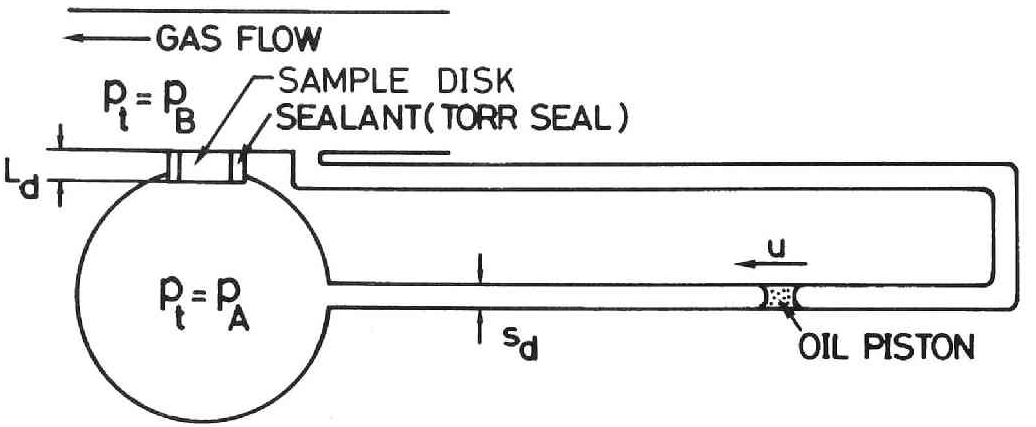

Fig. 3-4. Schematic diagram of diffusional experiment.

Eq. (3-9) in that interval.

$$j_A = \frac{p_t D_{ABe} A_d}{RT\gamma L_d} \ln\left[\frac{1 + (D_{ABe}/D_{KAe})}{1 - \gamma + (D_{ABe}/D_{KAe})}\right] \qquad (3\text{-}9)$$

where

$$\gamma = 1 - \sqrt{M_A/M_B}$$

The net flux equation is written as Eq. (3-10), because j_B can be rewritten as $-\sqrt{M_A/M_B} \cdot j_A$ using the Graham's law of diffusion [cf. Eq. (2-23)].

$$j_A(1 - \sqrt{M_A/M_B}) = (u\varepsilon_d p_t/RT) \qquad (3\text{-}10)$$

From Eqs. (3-9) and (3-10), the value of effective binary diffusivity D_{ABe} can be determined using the known value of D_{KAe}. Since the tortuosity factor, q, is obtained from a well known relation; $D_{ABe} = (\varepsilon/q)\, D_{AB}$, the effective binary diffusivity of water-vapor and air system, D_{vae}, is given by

$$D_{vae} = (\varepsilon/q)\, D_{va} = (D_{ABe}/D_{AB})\, D_{va} \qquad (3\text{-}11)$$

The dependency of binary diffusivity on temperature and total pressure is given by [7]

$$D_{va}(T,p_t) = D_{va}|_{T_0,p_{t0}} \left(\frac{T}{T_0}\right)^{1.75} \left(\frac{p_t}{p_{t0}}\right)^{1} \qquad (3\text{-}12)$$

The following expression is applicable to drying processes at an arbitrary temperature and total pressure.

$$D_{vae} = \frac{D_{ABe}}{D_{AB}} D_{va}|_{T_0,p_{t0}} \left(\frac{T}{T_0}\right)^{1.75} \left(\frac{p_t}{p_{t0}}\right)^{1} \qquad (3\text{-}13)$$

where

$$D_{va}|_{T_0=313K,p_{t0}=1.01\times10^5 Pa} = 2.77 \times 10^{-5}\ m^2 \cdot s^{-1}$$

CHAPTER 4 WATER TRANSFER COEFFICIENT IN HYGROSCOPIC MICROCAPILLARY-POROUS BODY

4.1 Introduction

The drying mechanism of an hygroscopic porous body with micro-capillaries is so complicated in comparison with that of a non-hygroscopic one that it has not been quantitatively analysed. In particular, the transport properties of water (moisture) in hygroscopic materials have been reported in only a few previous papers [3] [9] [10]. Moreover, it should be emphasized that the transport properties may be determined completely independent of any drying experiments.

In this thesis, the sum of surface flow coefficient and capillary-condensed water transfer coefficient defined by the moisture-content gradient is called the "water transfer coefficient". This coefficient has been measured so far with coexisting air [9] [10]. As it is difficult to estimate a water-vapor flux under such a condition, however, the reliability of those measured coefficients is deficient in the region of low moisture-content. Therefore, the water transfer coefficient is measured completely independent of drying experiment under a condition that air does not exist, and is interpreted by the model proposed in this thesis.

4.2 Experimental Apparatus and Procedure

The schematic figure of experimental process is illustrated in Fig. 4-1. The experimental procedure is as follows: Suppose a glass bulb to which a sealed hygroscopic porous body is attached through a cock under an isothermal condition, and only the water vapor and moisture exist. Initially the moisture content in the body and the vapor pressure in the glass bulb are in equilibrium; (p_{v1}, X_1). The cock is closed and the pressure in the bulb is reduced a little to p_{v0}. As soon as the cock is opened at $t = 0$, the moisture within the body begins to be desorbed (evaporated) from the sample surface, and then the vapor pressure in the bulb, $p_v(t)$, increases with time. Finally the isothermal system reaches a new equilibrium state (p_{v2}, X_2). If the moisture content always exists in equilibrium with the vapor pressure, the equilibrium state on the surface of body changes with time as shown in Fig. 4-1 (B), and the moisture-content profile in the body also changes as shown in Fig. 4-1 (C). Since both changes of the moisture content and vapor pressure are fairly small in the above-mentioned process, a linear relation is established as shown in Fig. 4-1 (B). The experiment followed this process is called the "differential-desorption method" in this thesis.

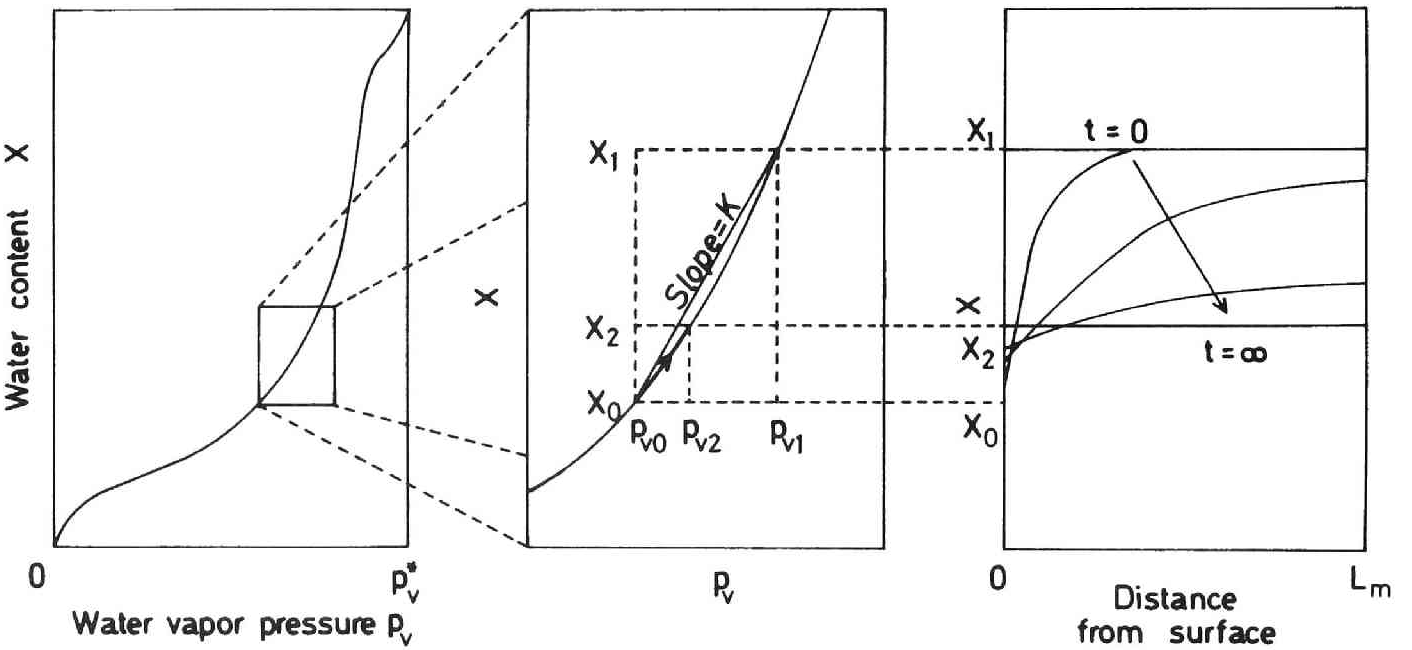

(A). Desorption isotherm. (B). Change of equilibrium state on sample surface. (C). Change of moisture content within sample.

Fig. 4-1. Schematic figure of experimental process.

The experimental apparatus is illustrated in Fig. 4-2. This apparatus is a modified form of that for the measurement of adsorption equilibrium using the constant-volume method, where Cock I in the drawing is the cock mentioned above. The sample used was an activated alumina, and it was a rectangular prism in shape and was set in the sample part (6). The pressure change in the system was continuously measured by the absolute pressure transducer (3).

The sample was coated with a low-vapor pressure resin (Torr Seal) with nickel powder, and the coated sample was embedded in a mixture of water glass and silver powder having high thermal conductivity, and a small vessel through which water at a constant temperature was circulated was attached to the rear of the mixture as shown in Fig. 4-3.

To prevent a lowering of temperature at the sample surface due to desorption, a fine thermocouple (C-A;100μm) was buried beneath the surface and a PID controller was used to regulate the radiant energy from a halogen lamp (5) so that the output signal of the thermocouple indicated a constant value in the whole range of t except in the initial period of desorption ($t < 60$s). The temperature of the sample was expected to be almost uniform and equal to that of the circulated water at $t \geq 60$s.

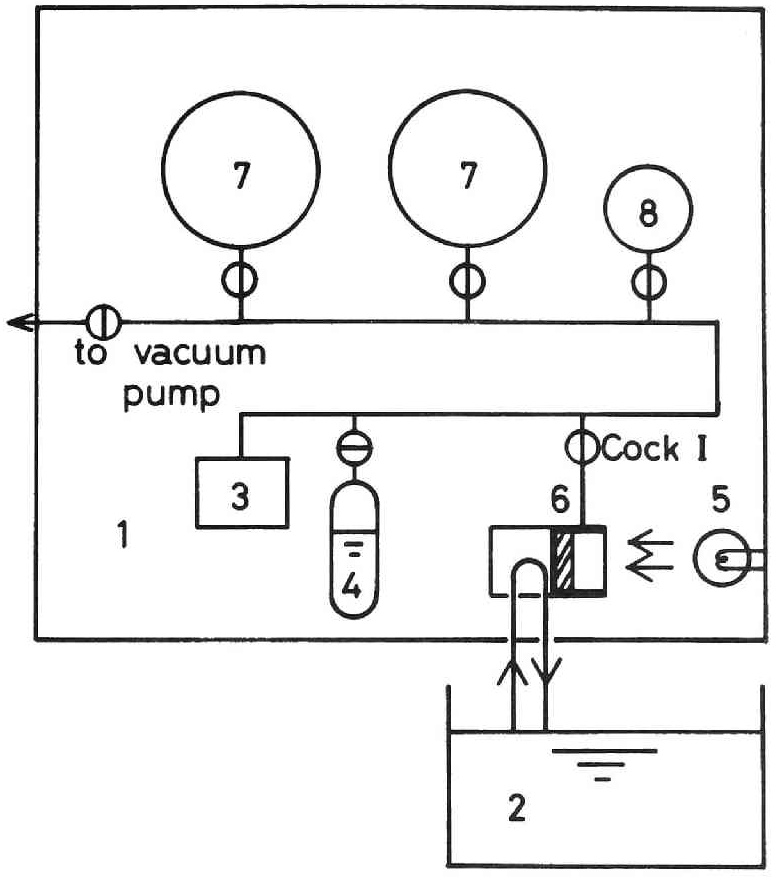

Fig. 4-2. Schematic diagram for differential desorption method. 1, constant-temperature box; 2, constant-temperature bath; 3, absolute pressure transducer; 4, water reservoir; 5, halogen lamp; 6, sample part; 7,8, glass bulb

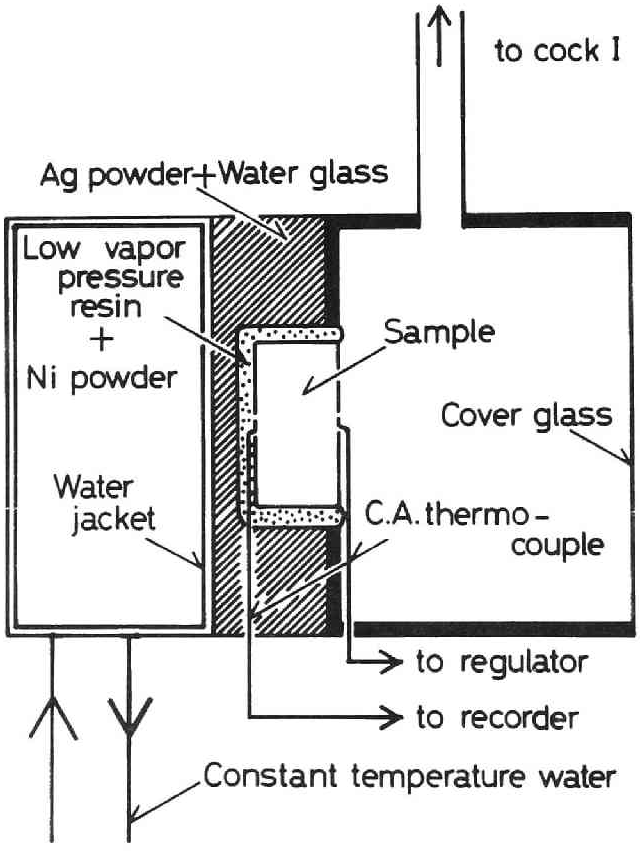

Fig. 4-3. Detailed drawing of sample part for differential desorption method.

The temperature in the constant-temperature box (1) was 3-4 degrees Celucius higher than that in the constant-temperature bath (2) to prevent the condensation of water vapor in the glass bulbs (7),(8).

Three samples, of different lengths and surface areas, were used as described later. These dimensions are shown in Table 4-1. Since the change of local moisture content in the sample between the initial and final states of the desorption experiment is small, the local equilibrium vapor pressure between them is assumed approximately to be a linear function of local moisture content. If the total water transfer coefficient, D_t, referred to the gradient in moisture content is assumed to be constant, D_t can be obtained from a curve of moisture desorption into evacuated surroundings with time between two equilibrium states under isothermal and vacuum conditions, and then the water transfer coefficient, D_w, can be obtained from the following relation.

$$D_w = D_t - D_v \tag{4-1}$$

where D_v is the vapor transfer coefficient referred to the gradient in moisture content and can be determined as

Table 4-1. Dimensions of samples

Sample	l_a [$\times 10^{-3}$ m]	l_b [$\times 10^{-3}$ m]	L_m [$\times 10^{-3}$ m]
I	1.5	1.8	10.7
II	2.3	2.3	6.0
III	5.7	5.8	1.2

Size of evaporation surface is l_a by l_b, and length is L_m.

described later. The process of moisture-content change in the sample can be written in the form of the following differential equation as

$$\frac{\partial X}{\partial t} = D_t \frac{\partial^2 X}{\partial y^2} \quad ; \quad X = K p_v + \frac{p_{v0}X_1 - p_{v1}X_0}{p_{v0} - p_{v1}} \tag{4-2}$$

$$K = (X_0 - X_1)/(p_{v0} - P_{v1})$$

where

$$\text{I. C.} \quad p_v = p_{v0}; \quad y = 0; \quad t = 0 \tag{4-3}$$

$$X = X_1; \quad 0 < y \leq L_m; \quad t = 0 \tag{4-4}$$

$$\text{B. C.} \quad \frac{v}{A_m \rho_{sapp} RT} \frac{M_v}{} \frac{\partial p_v}{\partial t} = - D_t \frac{\partial X}{\partial y} \; ; \; y = 0 \; ; \quad t > 0 \tag{4-5}$$

$$D_t \frac{\partial X}{\partial y} = 0 \; ; \; y = L_m \; ; \; t > 0 \tag{4-6}$$

where subscripts 0 and 1 represent the initial equilibrium state and $t = 0$, respectively, T is the temperature in the constant-temperature box (1), and D_t almost corresponds to the value at the temperature of circulated water. Equations (4-2) - (4-6) can be solved analytically [4], and the solution is given by

$$\begin{bmatrix}\text{Desorption amount of} \\ \text{moisture from sample} \\ \text{during time}\end{bmatrix} \quad \div \quad \begin{bmatrix}\text{corresponding} \\ \text{amount during} \\ \text{infinite time}\end{bmatrix}$$

$$= \frac{p_v(t) - P_{v0}}{p_{v2} - p_{v0}} = 1 - \sum_{n=1}^{\infty} \frac{2\alpha(1+\alpha)}{1+\alpha+\alpha^2\phi_n^2} \exp(-D_t\phi_n^2 t/L_m^2) \qquad (4\text{-}7)$$

where ϕ_n is the n-th positive root of the equation given as

$$\tan \phi_n = - \alpha \phi_n$$

where

$$\alpha = vM_v/(A_m \rho_{sapp} RTKL_m)$$

and p_{v2} is the vapor pressure of the glass bulb in the final equilibrium state. The total transfer coefficient of water can be obtained from the vapor pressure in the bulb at t seconds after, $p_v(t)$, using Eq. (4-7).

Since the purpose of the present study is to obtain the water transfer coefficient D_w, the vapor transfer coefficient D_v must be known in addition to D_t. As the vapor transport is represented as a sum of both the Kunudsen and viscous flow in this case, D_v is written as the following equation, if we set $dX/dp_v = K$ in Eq. (2-22).

$$D_v = \frac{M_v}{RT\rho_{sapp}K}\left(D_{Kve} + \frac{B_0}{\mu_v}\bar{p}_v\right)\left(1 - \frac{X}{X^*}\right) \qquad (4\text{-}8)$$

The viscous gas flow parameter B_0 and the effective Kunudsen diffusivity of Argon gas at 30 °C, $D_{KAre}|_{30°C}$, were obtained

using the results of the permeability measurement described in Section 3-2. Since D_{KAre} is proportional to $\sqrt{T/M}$, D_{Kve} and B_0 at T[K] become $7.360 \times 10^{-8} \cdot \sqrt{T}$ $m^2 \cdot s^{-1}$ and 3.81×10^{-16} m^2 ,respectively. So the value of D_v is determined at an arbitrary temperature. By repeating the above differential-desorption step successively, D_w in a wide range of X and the desorption isotherm in the same range can be obtained.

4.3 Results and Discussios

The activated alumina used for the experiment was supplied by Sumitomo Aluminium Smelting Co., Ltd. Its specific surface area is 1.30×10^5 $m^2 \cdot kg^{-1}$, saturated moisture content is 0.43, pore radius shows a distribution of about 2.5-18 nm, and apparent density ρ_{sapp} is 1381 $kg \cdot m^{-3}$. Cumulative pore-volume and surface-area distributions are drawn in Fig. 4-4. An experimental result of the desorption isotherm for the activated alumina at 30°C is shown in Fig. 4-5.

The moisture held in the material is the sum of both adsorbed water and capillary condensed water, and so the desorption isotherm can be correlated by the B.E.T. equation in the adsorbed region, and predicted by combining the cumulative pore-volume and surface-area distributions and

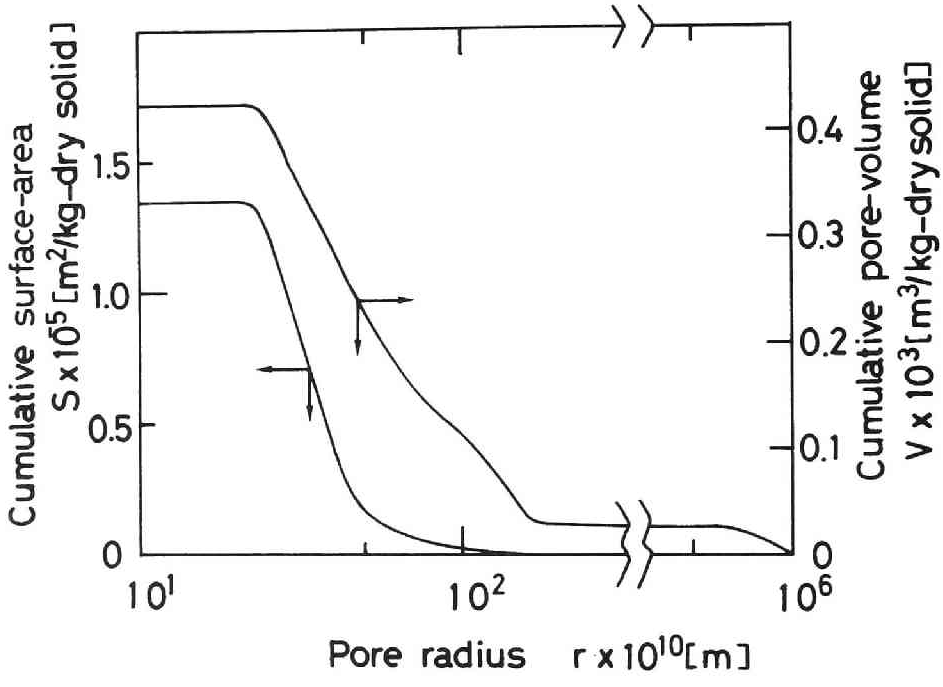

Fig. 4-4. Cumulative pore-volume and surface-area distributions of activated alumina.

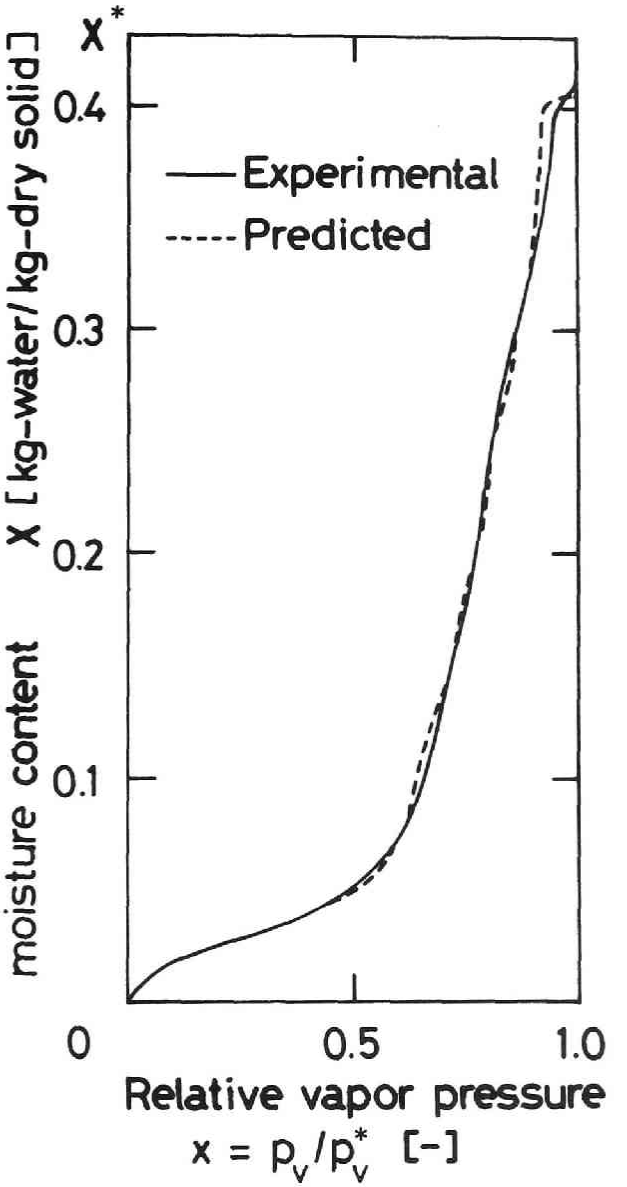

Fig. 4-5. Desorption isotherm of water for activated alumina. (30 °C)

the Kelvin equation in the condensed region, as is shown in Section 2.2. A comparison between the predicted curve and experimental data is illustrated in Fig. 4-5, and they agree well.

Examples of the value of vapor-pressure change observed by the absolute pressure transducer (3) with time are shown for three samples in Fig. 4-6. Each curves is the best fit of Eq. (4-7) to the experimental points by taking proper value of D_t. If the desorption process is caused under the isothermal condition and the observed vapor-pressure is controlled by the surface moisture-content of the sample in accordance with the isotherm, the curves are expected to agree with the observed value in the whole range of t. Since the agreements are good as shown in Fig. 4-6, it is verified that the proposed method is useful to determine the water transfer coefficient. The relationship between D_w at 30°C obtained from Eqs. (4-1), (4-7) and (4-8) and moisture content, X, is shown in Fig. 4-7.

Three samples having different dimensions (see Table 4-1) were used for measurement, in spite of being the same transport properties. When the longest Sample I was used, it took more than one day until the vapor pressure in the evacuated surroundings scarcely change at $X < 0.18$, and so

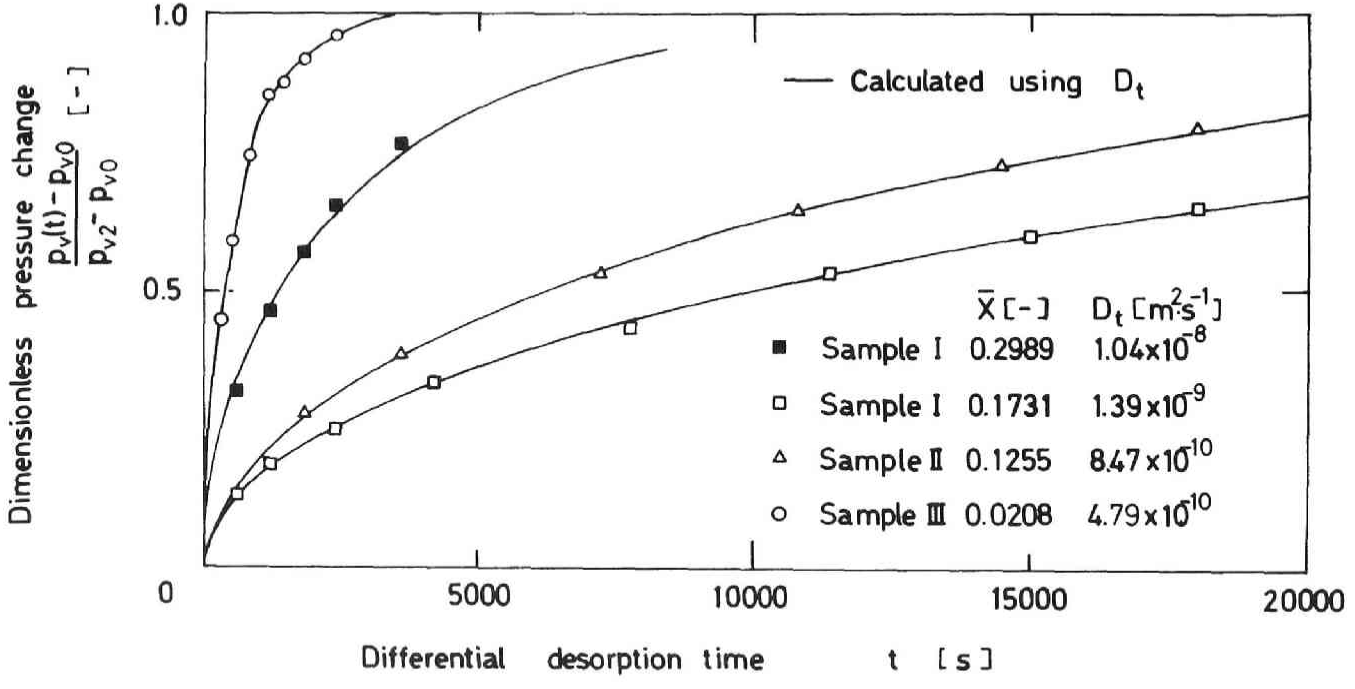

Fig. 4-6. Pressure change inside apparatus by differential desorption.

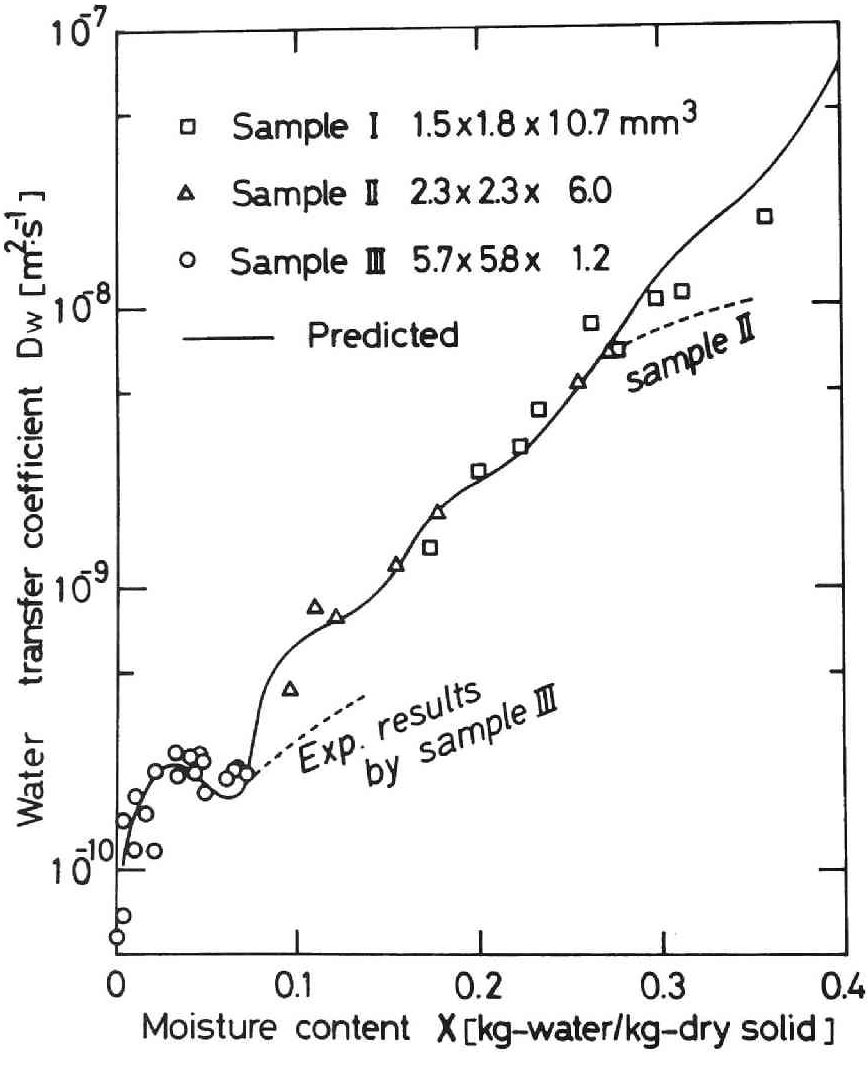

Fig. 4-7. Water transfer coefficient in activated alumina. (30 °C)

the amount of air leakage compared with that of desorbed moisture could not be ignored. In case of Sample II, which was shorter than Sample I, the value of D_w determined was smaller than those for Sample I at $X > 0.28$ and the fitting accuracy of D_t was less satisfactory. The reason is considered as follows: When D_w is large ($D_w > 7 \times 10^{-9}$ $m^2 \cdot s^{-1}$ in the case of Sample II), it seems the desorption rate of the sample surface is so large that the actual temperature at the surface falls, and so the desorption rate also decreases according to the equilibrium relationship shown in Fig. 4-5*. As it also took too much time to reach the equilibrium state at $X < 0.09$ in case of Sample II, the shortest Sample III was used. The value of D_w determined

---

* The following trial calculations were performed to verify the surmise mentioned above. If the volume of evacuate surroundings v is infinitely large, and the actual temperature at the surface is 0.5 °C lower than the initial value at t - 60 s and the moisture content on the surface changes with time as $\xi(t) = X_2 + (X_1 - X_2)e^{-\lambda t}$, where λ is a parameter related to the quality of the reduced temperature on the surface and the desorption isotherm, the author could simulate a tendency similar to the experimental results for Samples II ($X > 0.28$) and III ($X > 0.08$) shown in Fig. 4-7.

was also smaller than those for other samples at $X > 0.08$. The three samples, of different lengths as shown in Table 4-1, were needed to determine D_w for the whole range of X as a result. Consequently, it is concluded that only the experimental results giving good fitting-accuracy of D_t in the whole range of t as shown in Fig. 4-6 should be selected.

Experimental data have a minimum at $X = 0.07$ as shown in Fig. 4-7. This is because that D_w can be given by the sum of the adsorbed-water transfer coefficient, D_s, and the condensed-water transfer coefficient, D_l, and the detail is described in Section 6.5. These data can be utilized to determine both parameters in the correlating equations of adsorbed-water flow and condensed-water flow. In the region only the adsorption takes place, D_w becomes D_s in the absence of the capillary condensed water. On the other hand, in the region where the most of moisture content is the condensed water, D_w can be regarded as D_l. In the present case, the former region is equivalent to $X < 0.05$, and the latter $X > 0.15$. The two parameters, D_{s0} and a, related to the transport of the adsorbed water can be determined by the experimental data in the region of $X < 0.05$ using the following equation of Eq. (2-33),

$$D_s = D_{s0}\frac{(1-x)[\exp(-aE_{a0}/RT)-\exp(E_{a0}/RT)]}{[1-\exp(-E_{a0}/RT)]\{1-\theta(1-x)[1-(\tau_1/\tau_0)]\}}\left(\frac{S_s}{S_t}\right)\left(\frac{dX}{dX}\right)_B$$

and the value of parameters were given by

$$D_{s0} = 6.33 \times 10^{-7} \quad m^2 \cdot s^{-1}$$

$$a = 0.528$$

The propriety of the value for a set of parameters in the adsorption region will be discussed in CHAPTER 8. The experimental data of the condensed-water region of $X > 0.15$, on the other hand, were tried to correlate by the following equation of the original "modified Kozeny-Carman model" [cf. Eq. (2-30)][19][21]

$$D_l = D'_{l0}\left(\frac{T}{T_0}\right)\left(\frac{\mu_{l0}}{\mu_l}\right)\left(\frac{X_l}{X^*}\right)^3\left(\frac{S_t}{S_l}\right)^2\left(\frac{1}{p_v}\right)\left(\frac{dp}{dX}\right)_v$$

When the parameter, D'_{l0}, in the above equation was constant, the experimental data were not correlated successfully. Therefore, a plot of D'_{l0}, obtained from the experimental data, versus (X_l/X^*) is given in Fig. 4-8 to examine a dependency of D'_{l0} on the moisture content. This figure shows that the parameter D'_{l0} can be approximately proportional to (X_l/X^*). As the parameter D'_{l0} is written as the following form

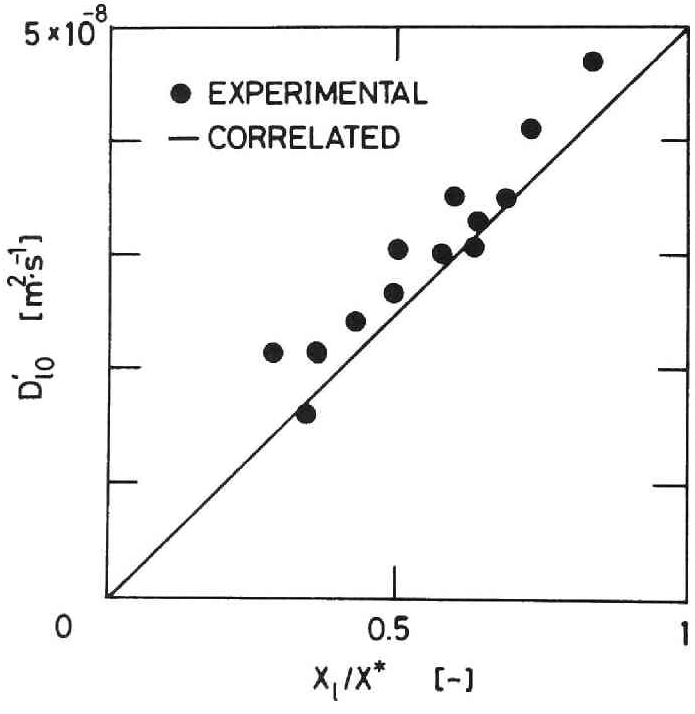

Fig. 4-8. D'_{l0} as a function of (X_l/X^*) .

$$D'_{l0} = \frac{RT_0(X^*)^3}{\rho_l K_c M_v S_t^2 \mu_{l0}}$$

and only the Kozeny constant in the above expression can be regarded as a variable with the moisture content, Fig. 4-8 shows that the dependency of the Kozeny constant on the moisture content is given by Eq. (2-31), as is mentioned in Section 2.4.

$$K_c = K_{c0} \ (X^*/X_l)$$

Consequently, the following correlating equation is derived [cf. Eq. (2-32)]

$$D_l = D_{l0} \left(\frac{T}{T_0}\right)\left(\frac{\mu_{l0}}{\mu_l}\right)\left(\frac{X_l}{X^*}\right)^4\left(\frac{S_t}{S_l}\right)^2\left(\frac{1}{p_v}\right)\frac{dp_v}{dX}$$

and the parameter D_{l0} in the equation was given by

$$D_{l0} = 4.01 \times 10^{-8} \ \mathrm{m^2.s^{-1}}$$

$$\text{at } T_0 = 303 \ \mathrm{K}, \quad \mu_{l0} = 8.16 \times 10^{-4} \ \mathrm{Pa.s}$$

A relationship between the experimental data and the curve predicted by use of the parameters at 30 °C is shown in Fig. 4-7. As the predicted curve is related to cumulative distribution functions and the desorption isotherm, it has a complicated figure. Since agreement between the experimental data and the predicted curve is satisfactory,

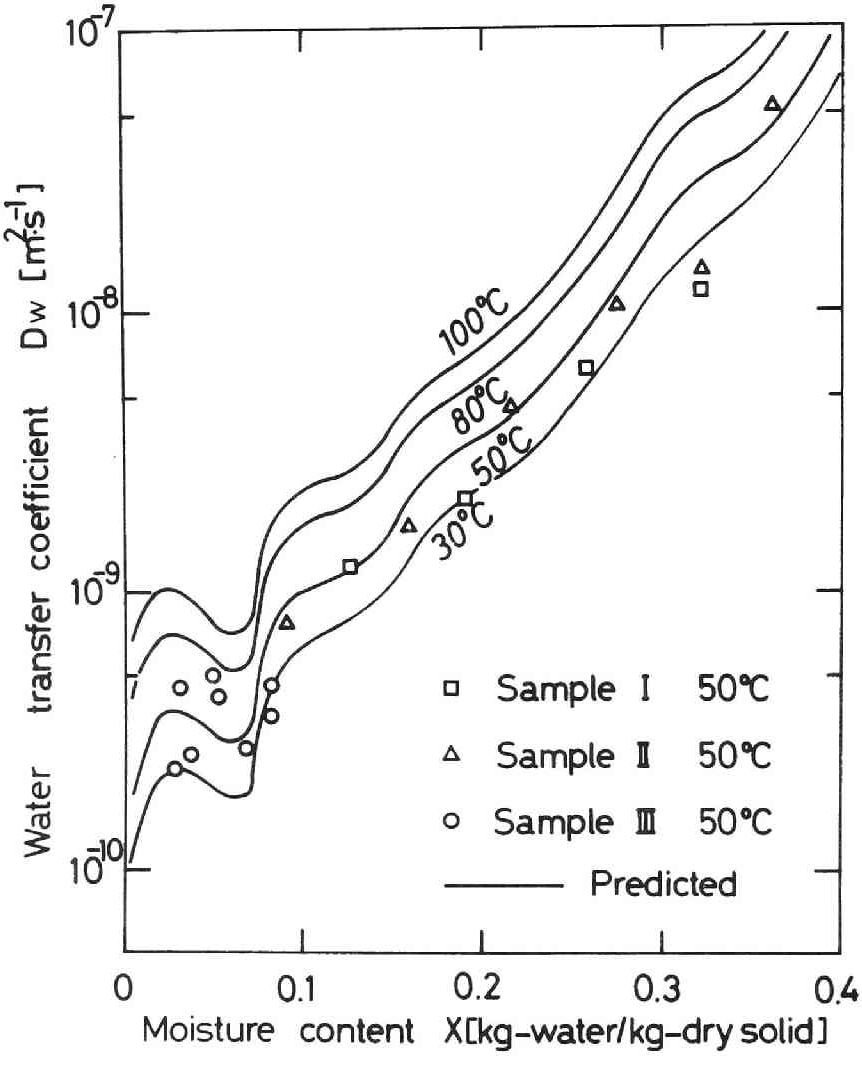

Fig. 4-9. Water transfer coefficient in activated alumina.

it can be said that the moisture content dependency on the water transfer coefficient is well interpreted by the proposed transfer model described in Section 2.4.

Fig. 4-9 shows the agreement between the experimental data and the predicted curve using the model at 50 ℃ in spite of scattering of the experimental data. The predicted curves at 30 ℃, 80 ℃, and 100 ℃ are also drawn in the same figure.

4.4 Conclusions

To clarify the drying mechanism of hygroscopic (adsorptive) porous bodies with micro-capillaries, the water transfer coefficient D_w for the activated alumina whose pores are fine was measured by use of the "differential-desorption method". The dependence of D_w on both moisture content and temperature was also observed. The experimental data were tried to explain using the "modified Kozeny-Carman model" for the capillary condensed water and the "modified hopping model" for the adsorbed water.

The conclusions in this chapter are as follows:

(1) A simple experimental method to measure D_w, which represents the sum of transport of adsorbed water and capillary condensed water in a short period is proposed,

using an easy but strict analysis.

(2) D_w in the range over a few order of magnitude was measured by changing only the sample length.

(3) A combination of the "modified hopping model" and the "modified Kozeny-Carman model" can explained successfully the experimental data, however the Kozeny constant in the "modified Kozeny-Carman model" was not a constant but a variable with the moisture content and was represented as the following way; $K_c \propto (X^*/X_l)$. The three parameters were introduced to the two correlating equations, and especially, the propriety of two parameters for the equation of the adsorption region will be discussed in CHAPTER 8.

(4) The results of experiment at temperatures of 30 - 50°C could be well interpreted by the model proposed.

The reliability of D_w obtained in this chapter is confirmed by comparison of simulation result using D_w with experimental one on a vacuum drying process in the next chapter.

CHAPTER 5 MOISTURE-CONTENT PROFILES FOR ACTIVATED ALUMINA ON ISOTHERMAL VACUUM-DRYING

5.1 Introduction

The "water transfer coefficient", representing the sum of transport of adsorbed water and capillary condensed water in wet hygroscopic (adsorptive) porous body, was observed by the "differential-desorption method" in CHAPTER 4. The reliability of the coefficient is examined by comparison of the experimental results of vacuum drying at a constant temperature with predicted results using an activated alumina rod as an example.

5-2 Fundamental Equations

In the drying of hygroscopic microcapillary porous body, the apparent flux of the total water is given by the sum of flux of the water vapor, the capillary condensed water, and the adsorbed water, when the system is isothermal and the transport is considered to be independent of one another.

$$J_t = J_v + J_l + J_s = J_v + J_w \qquad (5\text{-}1)$$

As the system does not contain air, the flux of the water

vapor is written as

$$J_v = -\rho_{sapp} D_v \frac{dX}{dy}$$

$$= -\frac{M_v}{RT}\left(D_{Kve} + \frac{B_0}{\mu_v}\right)\left(1 - \frac{X}{X^*}\right)\frac{dp_v}{dX}\frac{dX}{dy} \qquad (2\text{-}22)$$

The flux of the capillary condensed water and the adsorbed water is also given, respectively, by

$$J_l = -\rho_{sapp} D_l \frac{dX}{dy}$$

$$= -\rho_{sapp} D_{l0}\left(\frac{T}{T_0}\right)\left(\frac{\mu_l}{\mu_{l0}}\right)\left(\frac{X_l}{X^*}\right)^4\left(\frac{S_t}{S_l}\right)^2\left(\frac{1}{p_v}\right)\frac{dp_v}{dX}\frac{dX}{dy} \qquad (2\text{-}32)$$

$$J_s = \rho_{sapp} D_s \frac{dX}{dy}$$

$$= -\rho_{sapp} D_{s0} \frac{(1 - x)[\exp(-aE_{a0}/RT) - \exp(-E_{a0}/RT)]}{[1 - \exp(E_{a0}/RT)]\{1 - \theta(1 - x)[1 - (\tau_1/\tau_0)]\}}$$

$$\times (S_s/S_t)\frac{dX_B}{dX}\frac{dX}{dy} \qquad (2\text{-}33)$$

where

$$\tau_1/\tau_0 = \frac{[1 - \exp(-E_{a1}/RT)][\exp(-aE_{a0}/RT) - \exp(-E_{a0}/RT)]}{[1 - \exp(-E_{a0}/RT)][\exp(-E_{s1}/RT) - \exp(-E_{a1}/RT)]}$$

and the water transfer coefficient is defined by

$$D_w = D_l + D_s \qquad (5\text{-}2)$$

5.3 Experimental Apparatus and Results

The experimental apparatus used is illustrated in Fig. 5-1. The sample used was an activated alumina whose properties are the same as in CHAPTER 4 (see Table 5-1 and 5-2), and the shape was cylindrical (9ϕ x 18 mm). It was coated with a low-vapor pressure resin (Torr Seal) to hold vacuum except for the evaporation surface. The sample was set in a constant-temperature box and the temperature on the evaporating surface was not controlled. The vacuum drying curve was obtained from tracing the weight change of the sample with time. The relationship between the averaged dimensionless moisture content of the sample and time is shown in Fig. 5-2. The pore radius of the sample is so small that the activated alumina possesses no constant drying-rate period.

Another experiment was performed to obtain moisture-content profiles with time using samples of the same dimensions as above-mentioned one. After a prescribed drying time, the sample was taken out of the constant-temperature box and quickly cut, into five or six pieces parallel to the drying surface, in the atmosphere. The moisture content of these pieces was obtained by drying them in a vacuum dryer for two days at 60°C. The relationship between the moisture-content

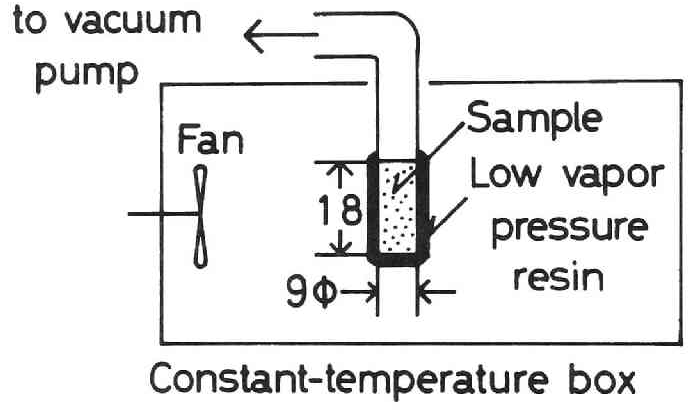

Fig. 5-1. Experimental vacuum drying apparatus.

Table 5-1. Properties of activated alumina

Apparent density	ρ_{sapp}	1.38×10^{3}	$kg \cdot m^{-3}$
Specific surface area	S_t	1.30×10^{5}	$m^2 \cdot kg^{-1}$
Saturated moisture content	X^*	0.43	
Pore radius distribution	r	$25 - 180 \times 10^{-10}$	m

Table 5-2. Transport properties of activated alumina

D_{Kve}	$7.36 \times 10^{-8}\sqrt{T}$	$m^2 \cdot s^{-1}$
B_0	3.81×10^{-16}	m^2
D_{s0}	6.33×10^{-7}	$m^2 \cdot s^{-1}$
a	0.528	
D_{l0}	4.01×10^{-8}	$m^2 \cdot s^{-1}$

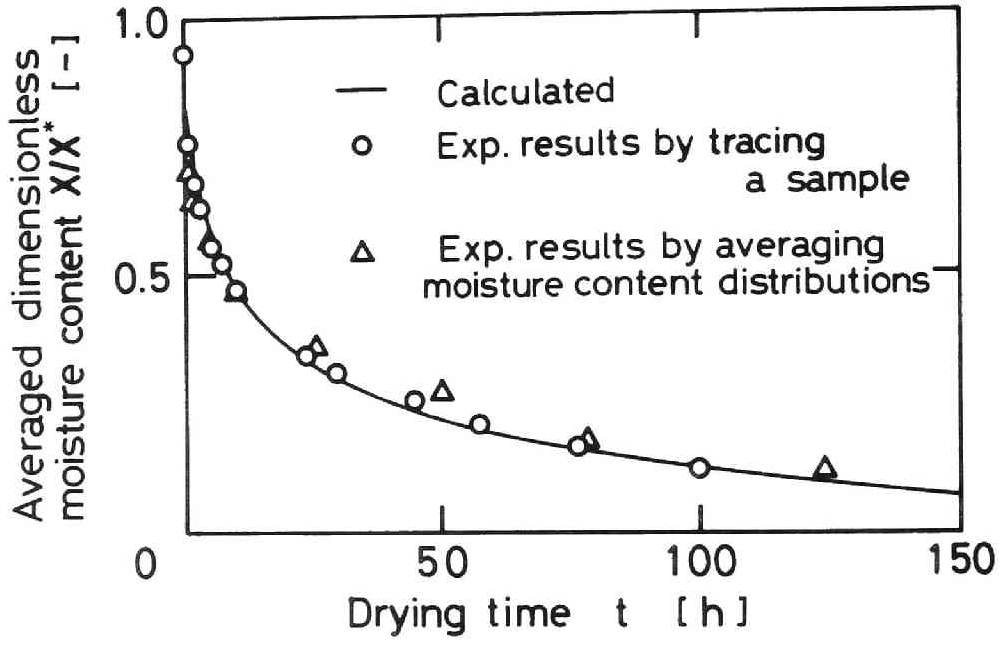

Fig. 5-2. Drying curve of activated alumina.
($30\,^{\circ}C$; $L = 1.80 \times 10^{-2}$ m)

distributions and dimensionless distance from the drying surface is shown in Fig. 5-3 using time as a parameter, and the averaged dimensionless moisture content obtained from the distributions are shown in Fig. 5-2. Each piece of the sample is small (dry solid 0.2 g) in size. During the time required to cut the sample into small pieces, though it is within a few minutes, some amount of moisture in the pieces supposedly evaporated away at a high moisture content, and some amount of atmospheric water vapor was adsorbed at a low moisture content. As a result, the experimental data scatter in this case, and the moisture-content profiles in Fig. 5-3 seem a little difference from the actual ones.

5.4 Numerical Results

When the isothermal assumption in the system is valid during vacuum-drying and the evaporation resistance of water on the surface is ignored, the mass-transfer rate in the y direction within a wet porous slab is given by,

$$\frac{\partial X}{\partial t} = \frac{\partial}{\partial y}\left(D_v + D_w\right)\frac{\partial X}{\partial y} \qquad (5\text{-}3)$$

I. C. $X = X^*$; $0 \leq y \leq L$; $t = 0$ (5-4)

B. C. $X = 0$; $y = 0$; $t > 0$ (5-5)

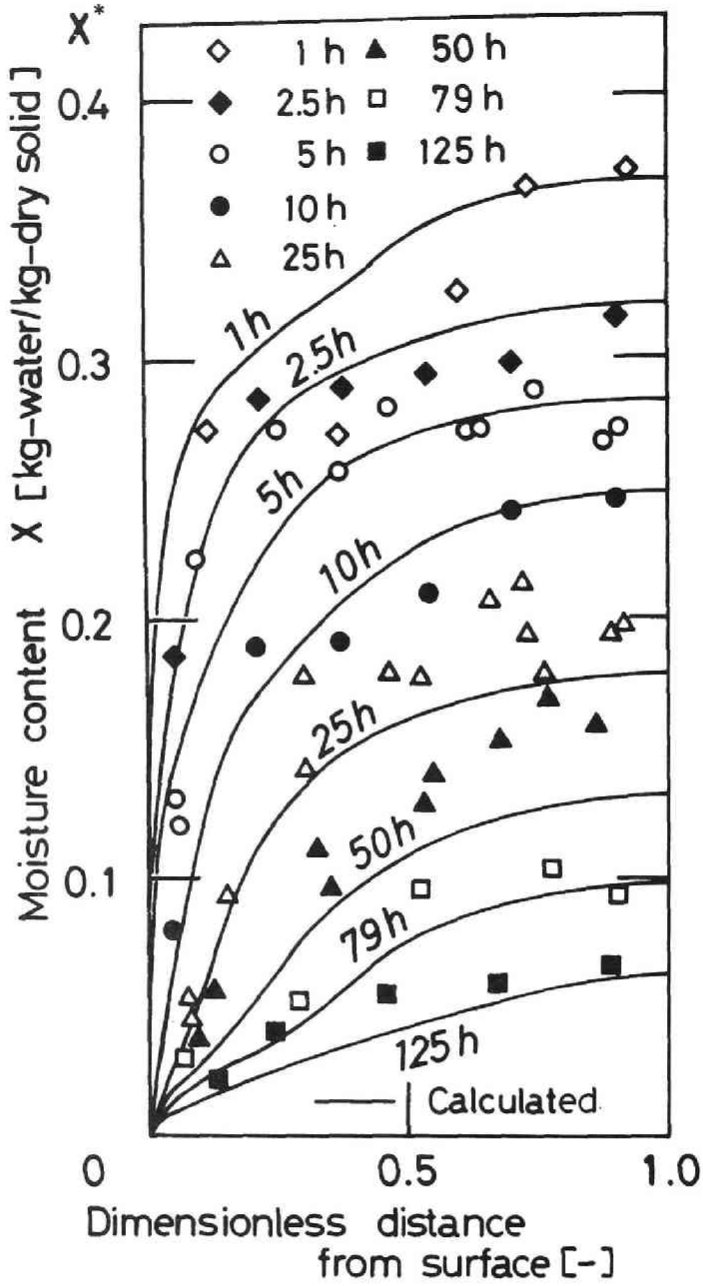

Fig. 5-3. Moisture-content profiles in activated alumina. (30 °C; L 1.80 x 10^{-2} m)

$$(D_v + D_w)\frac{\partial X}{\partial y} = 0;\ y = L\ ;\ t > 0 \qquad (5\text{-}6)$$

where L [m] is the length of the sample. D_w in Fig. 4-7 in CHAPTER 4, which was measured by the differential desorption method, and D_v calculated by Eq. (2-22) were used for calculation of the moisture-content profiles. Since $D_w + D_v$ is a function of the moisture content, it is impossible to obtain an analytical solution of the above equations and thus the implicit method was used to solve Eqs. (5-3) - (5-6) numerically.

As the temperature drop at the evaporating surface at the initial period of the drying was about equal to but more than 3 degrees Celsius according to the temperature measurement, its effect on the drying rate was ignored.

The calculated result of drying curve with time is given by a solid line shown in Fig. 5-2. The curve agrees well with the experimental value . The calculated curves for the moisture-content profiles with time are shown as solid lines in Fig. 5-3. Both the calculated curves and the experimental results show similar tendencies, although the experimental ones involve errors previously described.

5.5 Conclusions

Experiments in the vacuum drying of activated alumina at a constant temperature were performed and the reliability of the water transfer coefficient introduced in CHAPTER 4 was confirmed by comparing the experimental drying data with the calculated value .

CHAPTER 6 MOISTURE-CONTENT AND TOTAL-PRESSURE PROFILES FOR ACTIVATED ALUMINA ON ISOTHERMAL CONVECTION-DRYING

6.1 Introduction

This chapter deals with a examination of all the proposed mathematical expressions introduced in CHAPTER 2 and the measurement techniques of the transport properties and the pore structure characteristics introduced in CHAPTER's 3 and 4. The expressions and the techniques are applied to a hygroscopic microcapillary porous material on an isothermal convection-drying process.

6.2 Fundamental Equations

The flux of total water transfer is written as the following equation in this chapter as well as in CHAPTER 5.

$$J_t = J_v + J_s + J_l = J_v + J_w \tag{5-1}$$

As the gas phase within hygroscopic porous bodies in a convection drying contains the two components of water vapor and air, the flux of vapor is given by Eq. (2-21) for the case where the vapor pressure is controlled by the moisture content in accordance with a desorption isotherm as is

described in Section 2.3.

$$J_v = -\rho_{sapp} D_v \frac{dX}{dy} \tag{2-21}$$

$$= -\frac{M_v}{RT} D_{Kve}\left[1 + \left(\frac{p_v}{D_{Kve}} + \frac{p_t - p_v}{D_{Kae}}\right)\frac{B_0}{\mu_{mix}}\right]\left(1 - \frac{X}{X^*}\right)\frac{dp_t}{dp_v}\frac{dp_v}{dX}\frac{dX}{dy}$$

where

$$\frac{dp_t}{dp_v} = \frac{D_{ae} - \dfrac{D_{ae}(D_{ve} - D_{ae})(p_t - P_v)}{(D_{vae} - D_{ae})p_t + (D_{ae} - D_{ve})p_v}}{D_{ae} + \dfrac{(D_{ae})^2(p_t - p_v)}{(D_{vae} - D_{ae})p_t + (D_{ae} - D_{ve})p_v} + \dfrac{B_0}{\mu_{mix}}(p_t - P_v)} \tag{2-19}$$

The treatment of the adsorbed-water and the capillary condensed water flux is the same as in CHAPTER 5, namely

$$J_s = -\rho_{sapp} D_s \frac{dX}{dy}$$

$$= -\rho_{sapp} D_{s0} \frac{(1 - x)[\exp(-aE_{a0}/RT) - \exp(-E_{a0}/RT)]}{[1 - \exp(E_{a0}/RT)]\{1 - \theta(1 - x)[1 - (\tau_1/\tau_0)]\}}$$

$$\times (S_s/S_t)\frac{dX_B}{dX}\frac{dX}{dy} \tag{2-33}$$

$$J_l = -\rho_{sapp} D_l \frac{dX}{dy}$$

$$= -\rho_{sapp} D_{l0}\left(\frac{T}{T_0}\right)\left(\frac{\mu_{l0}}{\mu_l}\right)\left(\frac{X_l}{X^*}\right)^4\left(\frac{S_t}{S_l}\right)^2\left(\frac{1}{p_v}\right)\frac{dp_v}{dX}\frac{dX}{dy} \tag{2-32}$$

and the water transfer coefficient is also defined by

$$D_w = D_s + D_l \tag{5-2}$$

6.3 Physical Characteristic and Transport Properties of Drying Material

The material employed here is an activated alumina. Its apparent density $\rho_{sapp}$was 930 $kg \cdot m^{-3}$. Fig. 6-1 shows the cumulative distribution functions of pore-volume and surface-area. These results were obtained from combining the results of the mercury penetration and nitrogen sorption-condensation techniques. The pore radius mainly distributes 2.5 nm - 30 nm, and some huge pores ($\simeq$50 μm) coexist. This distribution range is about two times as large as the activated alumina used in CHAPTER's 4 and 5.

Fig. 6-2 shows a comparison of the predicted desorption curve with the experimental one of the desorption isotherm at 30°C. The predicted one was obtained from the curves in Fig. 6-1, the B.E.T. equation, and the Kelvin equation. Though the experimental data are not so precise in the region of x > 0.9, it can be said that the agreement between them is good.

This desorption isotherm can be interpreted from the physical viewpoint as follows; as the relative vapor pressure, x , increases, water molecules are adsorbed at

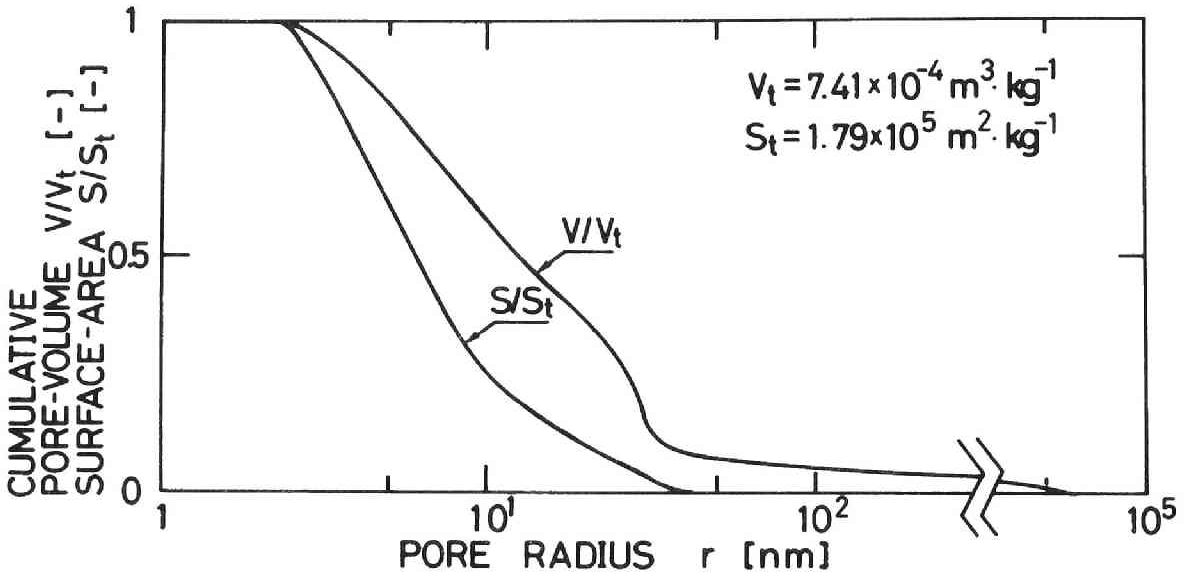

Fig. 6-1. Cumulative pore-volume and surface-area distributions.
(activated alumina)

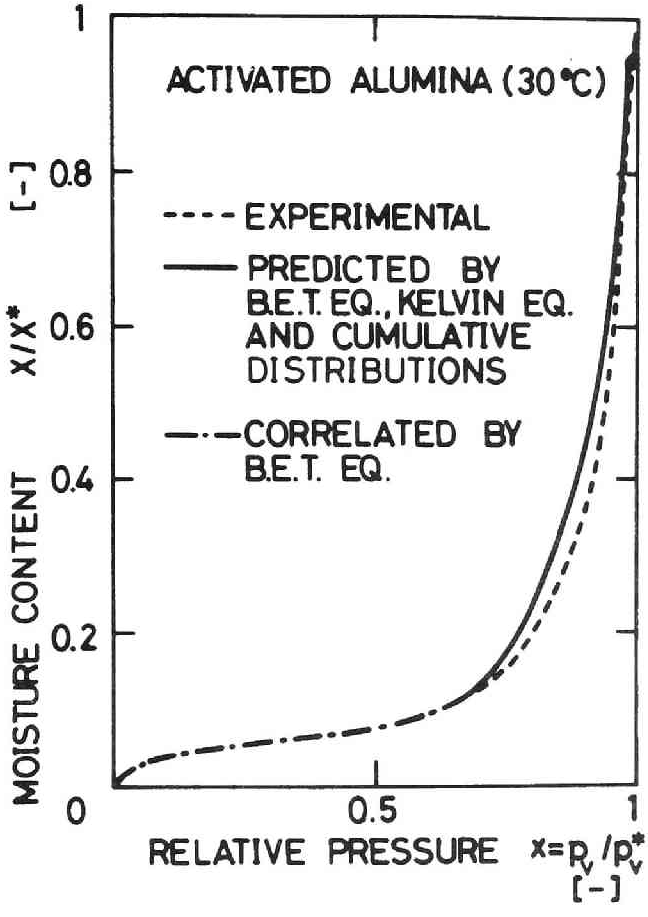

Fig. 6-2. Desorption isotherm of activated alumina. (30 °C); Experimental data below the relative pressure of 0.7 were correlated by the B.E.T. equation satisfactorily.

first in monolayer ($0 < x \leq 0.3$) and then in multilayer ($0.3 < x \leq 0.7$). The capillary condensation occurs above $x = 0.7$.

The water transfer coefficient defined by the sum of coefficients of the surface flow and the capillary-condensed water flow; $D_w = D_s + D_l$, was measured by the differential desorption method described in CHAPTER 4. Fig. 6-3 shows experimental data of the water transfer coefficient at 30°C. These data can be utilized to determine the both parameters in the correlating equations of surface flow and capillary-condensed water flow, as is described in Section 4.3. Consequently the following three parameters are given by

$$D_{s0} = 1.78 \times 10^{-5} \ m^2 \cdot s^{-1}$$

$$a = 0.64$$

$$D_{l0} = 5.24 \times 10^{-6} \ m^2 \cdot s^{-1}$$

$$\text{at } T_0 = 303 \text{ K}, \ \mu_{l0} = 8.16 \times 10^{-4} \ \text{Pa} \cdot \text{s}$$

The propriety of the value of a set of parameters of D_{s0} and a will be discussed in CHAPTER 8. A comparison between the experimental data and the curve predicted using the parameters at 30°C, and the predicted curve at 81.5°C are shown in Fig. 6-3.

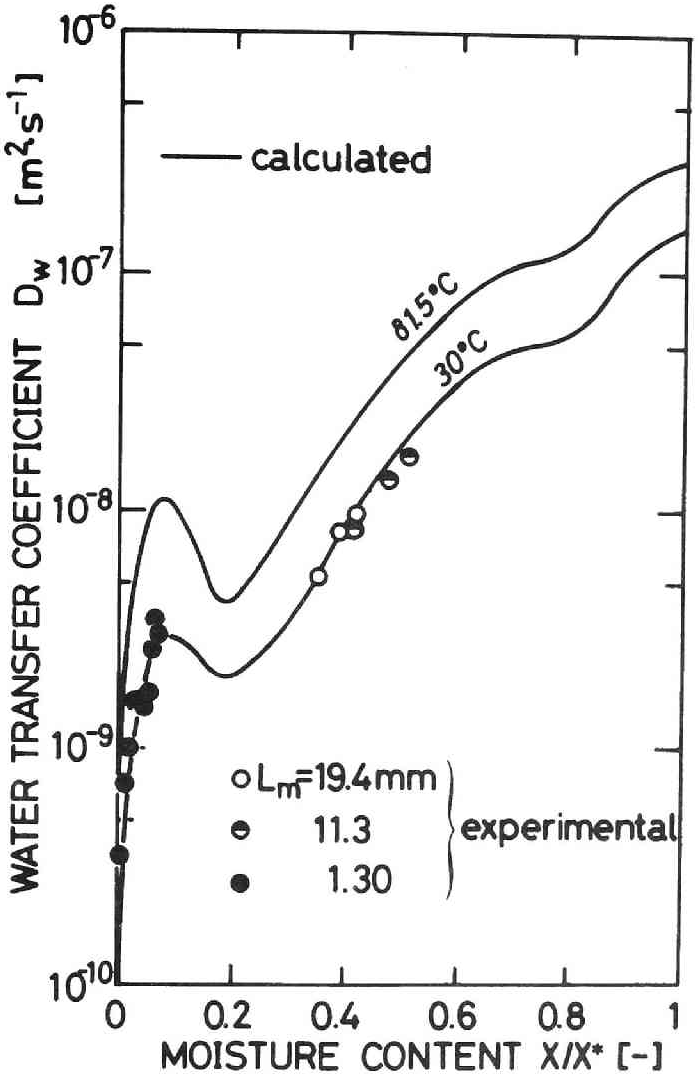

Fig. 6-3. Water transfer coefficient as a function of moisture content. (activated alumina)

The effective Kunudsen diffusivity and the viscous gas flow parameter are determined from the permeability measurement using steady-state method mentioned in Section 3.2, and the following expressions are applied at an arbitrary temperature.

$$D_{Kve} = 1.76 \times 10^{-7} \sqrt{T} \ \mathrm{m}^2.\mathrm{s}^{-1}$$

$$D_{Kae} = 1.39 \times 10^{-7} \sqrt{T} \ \mathrm{m}^2.\mathrm{s}^{-1}$$

$$B_0 = 6.00 \times 10^{-17} \ \mathrm{m}^2$$

The effective binary diffusivity is determined from the uniform-pressure diffusion measurement mentioned in Section 3.3, and the next expression is applicable to the drying process of this material at an arbitrary temperature and total pressure.

$$D_{vae} = 6.20 \times 10^{-16} \ T^{1.75} \ p_t^1 \ \mathrm{m}^2.\mathrm{s}^{-1}$$

where the next value is used ; $\varepsilon = 0.704$ and $q = 14.0$

6.4 Experimental Apparatus and Results

The experimental apparatus is illustrated in Fig. 6-4. The sample used was the activated alumina, and it was a rectangular prism in shape ($3 \times 3 \times 26$ mm^3). It was coated

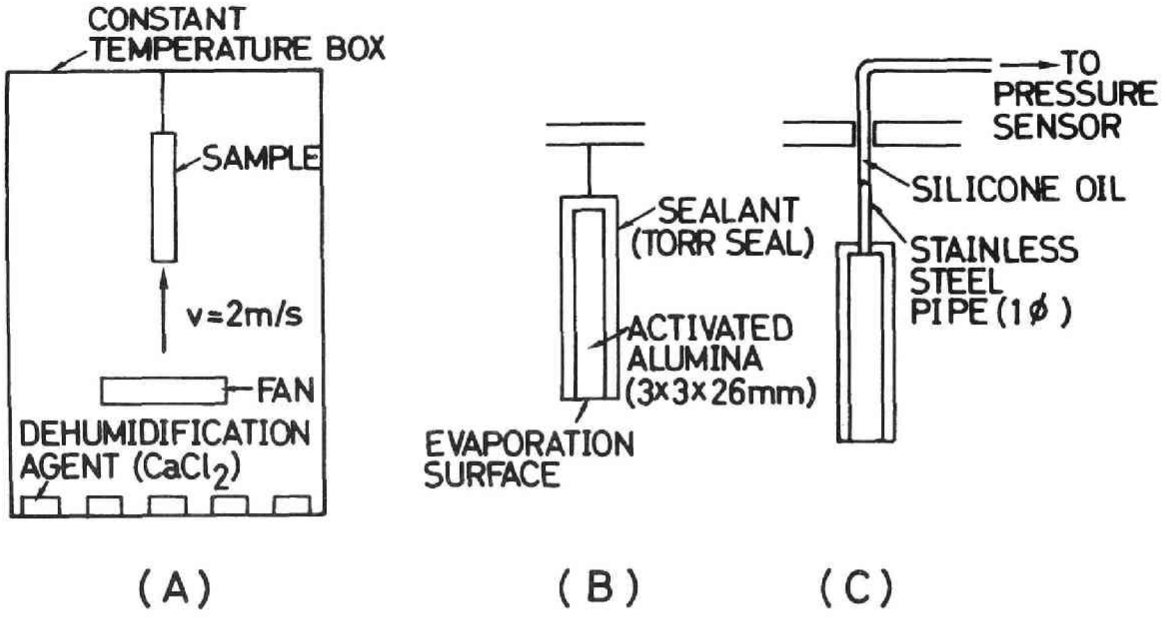

Fig. 6-4. (A). Schematic illustration of experimental apparatus of isothermal convection drying, (B). Sample of measurement for moisture-content profiles, (C). Sample of measurement for generated total pressure.

with a low vapor pressure resin (Torr Seal) except for the evaporating surface. The sample was set in a constant-temperature box (81.5 °C) as shown in Fig. 6-4 (A). A fan blowing hot air to the evaporating surface and the dehumidification agent on trays are attached in the box, and the velocity of air was 2 $m \cdot s^{-1}$ and the relative humidity was nearly zero in the box.

The two experiments were performed. One is to obtain the moisture-content profile with time and the other is to observe the total pressure in the sample. After a prescribed drying time, the sample was taken out of the box and quickly cut into five pieces parallel to the drying surface: Fig. 6-4 (B). The moisture content of these pieces was observed by drying them in a vacuum dryer for two days at 60 °C. The moisture-content profiles are shown in Fig. 6-5, and the averaged moisture contents obtained from the profiles are in Fig. 6-6.

The generated pressure in the sample was observed using a small size differential pressure transducer as shown in Fig. 6-4 (C). The sample was connected to the transducer by the stainless steel pipe of outer diameter 1 mm filled with a silicone oil to prevent the condensation of vapor in it.

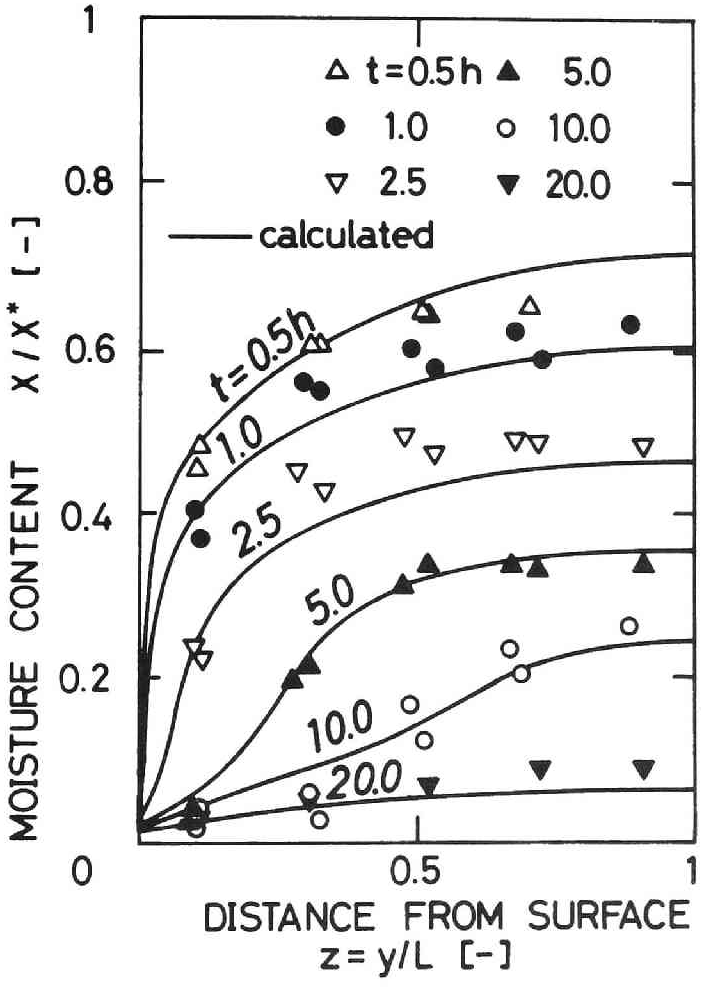

Fig. 6-5. Moisture profiles of activated alumina on isothermal convection drying. (81.5 °C)

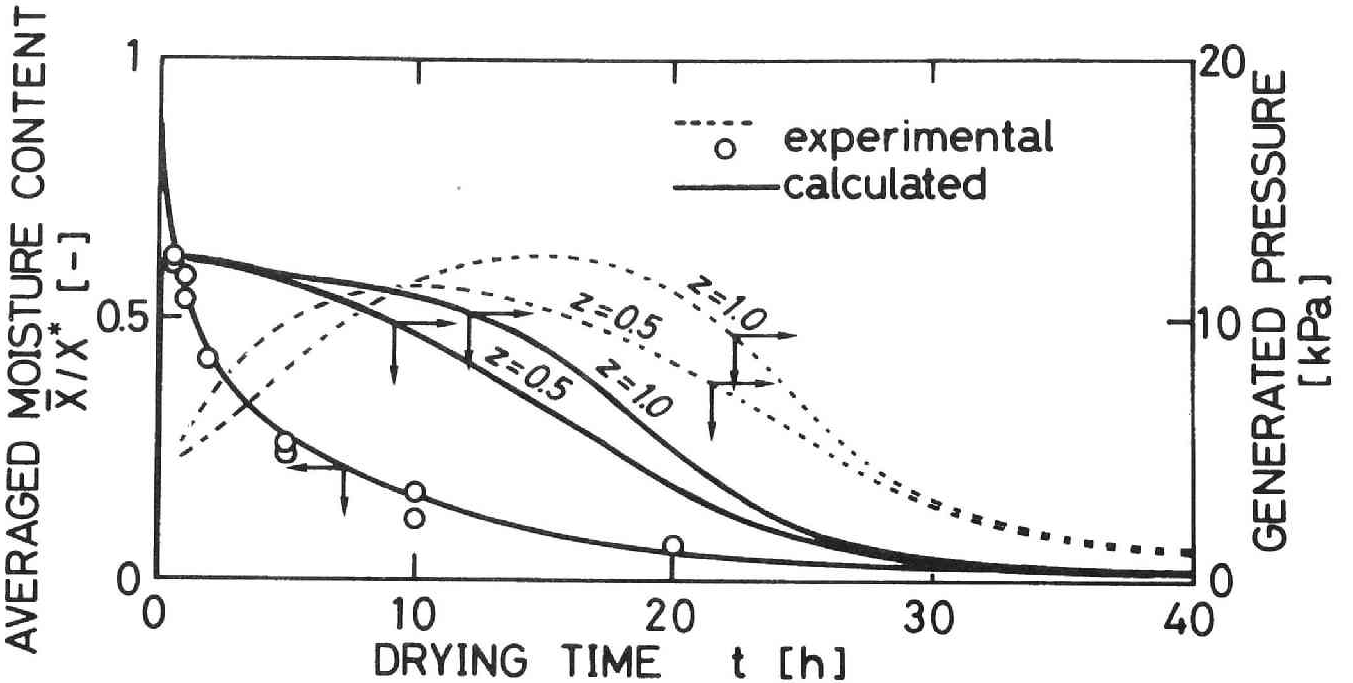

Fig. 6-6. Drying curve and generated pressures as a function of time for activated alumina on isothermal convection-drying. (81.5 °C)

The positions of the pressure measurement were z = 0.5 and z - 1. The changes of the generated pressures against time are given in Fig. 6-6. The temperature of the sample was equivalent to that of the hot air at t > 0.5 h, and so the drying process was deemed isothermal.

6.5 Numerical Results and Discussions

On the drying of the hygroscopic (adsorptive) microcapillary-porous material, the coefficient of total water transfer is given as the sum of coefficients of vapor transfer, surface flow and capillary condensed water flow, when the system is isothermal and these transfers are independent of one another, and then the mass transfer rate in the y direction in a wet porous slab is given by

$$\frac{\partial X}{\partial t} = \frac{\partial}{\partial y}(D_v + D_s + D_l)\frac{\partial X}{\partial y} \tag{6-1}$$

The initial condition is

$$X = X^*; \qquad 0 \leq y \leq L; \qquad t = 0 \tag{6-2}$$

The boundary conditions are

$$\frac{\partial}{\partial t}\int_0^L \rho_{sapp} X dy = k_g(p_v|_0 \quad p_{v(\text{hot air})}); \qquad 0 < t \tag{6-3}$$

$$(D_v + D_s + D_l)\frac{\partial X}{\partial y} = 0; \qquad y = L; \qquad 0 < t \tag{6-4}$$

Since D_v, D_s, and D_l in Eqs. (6-1) and (6-4) are the functions of the moisture content, X, the partial vapor pressure, p_v, and/or the total pressure, p_t, the profiles of p_v and p_t within the material have to be known in the calculation process. The partial vapor-pressure profile is directly governed by the moisture-content profile through the desorption isotherm. The total-pressure profile, on the other hand, is determined by solving numerically Eq. (2-19) which can be written in the following way:

$$\frac{dp_t}{dp_v} = f(p_t, p_v) \tag{6-5}$$

The boundary condition is

$$p_t|_0 = 1.01 \times 10^5 \text{ Pa (atmospheric pressure)} \tag{6-6}$$

The moisture content as a function of time and location was calculated from Eqs. (6-1) - (6-6). These equations were solved numerically by the use of the implicit finite difference technique. The calculation method is attributed to the problem to find the surface moisture content at $t = t + \Delta t$ by trial and error. The value of k_g was determined experimentally by performing a drying experiment of non-

hygroscopic material in the same condition as this case, but this value of k_g did not have an effect on the moisture-content profiles. This is because the drying material did not possess the constant drying rate period.

Figures 6-5 and 6-6 give comparisons of the simulation results and experimental results. Agreements between the calculated results and the experimental ones for the moisture content against time and position and for the drying curve are fairly good in spite of the smallness of sample size.

The calculated results of the generated pressure with time are shown by solid lines in Fig. 6-6. The agreement between the experimental data and the calculated results is not fairly good, but the both maximum values of two series of experiments can be predicted by the calculation method

Fig. 6-7 shows the variations of the calculated results of the total water transfer coefficient, D_t and the contribution of each coefficient, D_v, D_s, or D_l to D_t with moisture content. The transfer rate in the region of $X/X^* < 0.3$ is governed by the condensed water flow, and in the region of $X/X^* < 0.13$, on the other hand, is governed by the both transport of surface adsorbed water and vapor.

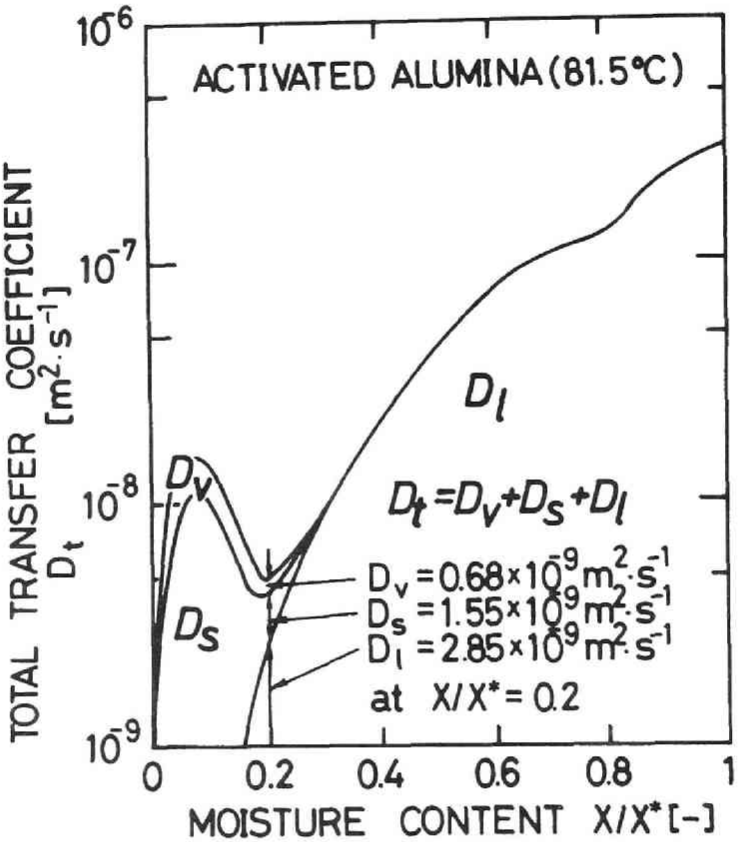

Fig. 6-7. Contribution of each coefficient to total transfer coefficient. (calculated)

The curve of D_t has the minimum at $X/X^* \simeq 0.2$. The reason is thought to be as follows considering Eqs. (4-9) and (4-10). The coefficient of condensed water D_l has the value of zero initially, and increases roughly exponentially from $X/X^* = 0.13$ with moisture content in accordance with Eq. (4-10), because the vapor condensation in the micro-capillaries begins to takes place at this moisture content. The surface flow coefficient D_s, on the other hand, decreases with increasing X_l because of the decreasing of the surface area S_s in Eq. (4-9). Since D_l is small compared with D_s in the region of $0.13 < X/X^* < 0.19$, the water transfer coefficient, $D_w = D_s + D_l$, decreases in this region. D_w increases gradually, however, with moisture content, because the increasing rate of D_l is greater than the decreasing one of D_s in the region of $X/X^* > 0.19$.

Though the agreement of the maximum generated pressures between the results of experiment and prediction is satisfactory, the variations of the generated pressures with time do not agree well. This fact seems to mean the rate of viscous vapor flow does not seriously have an effect on the drying rate. Accordingly, the vapor flux of the proposed drying model is compared with that from the uniform-pressure

diffusion.

The vapor flux of the model in this thesis is written as

$$J_v = - \frac{M_v D_{Kve}}{RT}\left[1 + \left(\frac{p_v}{D_{Kve}} + \frac{p_t - p_v}{D_{Kae}}\right)\frac{B_0}{\mu_{mix}}\right]\left(1 - \frac{X}{X^*}\right)\frac{dp_t}{dp_v}\frac{dp_v}{dy} \quad (2\text{-}21)$$

where dp_t/dp_v is given by Eq. (2-19). The vapor flux at the uniform-pressure diffusion is given as Eq. (6-7) as shown in Section 2.3.

$$J_v(\text{uniform-pressure}) = - \frac{M_v D_{Kve}}{RT}\left[\frac{D_{vae}}{D_{vae} + \frac{p_t - p_v}{p_t}D_{Kve} + \frac{p_v}{p_t}D_{Kae}}\right]\left(1 - \frac{X}{X^*}\right)\frac{dp_v}{dy} \quad (6\text{-}7)$$

Since the profiles of partial vapor pressure is governed by those of moisture content, the ratio of Eq. (6-7) to Eq. (2-21) is directly linked to a difference of drying rate.

$$\frac{J_v(\text{uniform-pressure})}{J_v} = \Omega(p_v, p_t, T) \quad (6\text{-}8)$$

Fig. 6-8 shows the relationship between p_v and Ω, where J_v(uniform-pressure) is calculated under the condition of atmospheric pressure, p_t 1.01 x 10^5Pa, and the given temperature T 354.7 K (81.5°C). J_v, on the other hand, is calculated at p_t 1.13 x 10^5Pa, namely the maximum

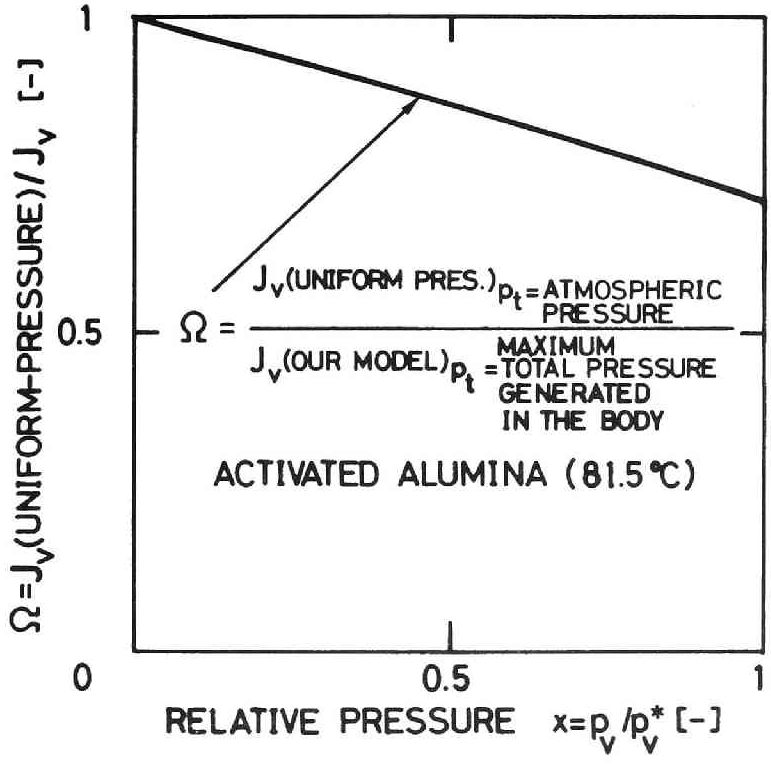

Fig. 6-8. Ratio of J_v(uniform-pressure) to J_v as a function of partial vapor pressure.

generated pressure, and T =354.7 K. The value of dp_t/dp_v varies from 0.25 at p_v = 0 to 0.35 at $p_v = p_v^*$ in this calculation. The ratio Ω reaches about 0.75 at X/X^* = 0.3 or x (p_v/p_v^*) = 0.85 from the desorption isotherm, where D_v does not have an effect on D_t any longer. Since the contribution of vapor flux to the total one is about 30 percent at most in the region of $X/X^* < 0.3$, the maximum error of J_t(uniform-pressure), which is the total flux at the uniform-pressure diffusion, to J_t, the total flux of the proposed model, is estimated as $(1 - \Omega|_{X/X^*=0.3})$ x (0.30) = 0.075.

6.6 Conclusions

The drying curve and the moisture-content profiles of the activated alumina, which is a hygroscopic micocapillary-porous material, on an isothermal convection-drying process were predicted well using the mathematical expressions of the isothermal drying process and the transport properties determined completely independent of any drying experiments. Though the agreement of change for generated total pressure with drying between the experimental data and the predicted one was less satisfactory, the effect of the disagreement on the drying rate was not serious.

CHAPTER 7 APPLICATION OF PROPOSED MATHEMATICAL MODEL TO ISOTHERMAL CONVECTION-DRYING OF NON-HYGROSCOPIC CAPILLARY-POROUS BODY

7-1 Introduction

The modified Kozeny-Carman equation originating from the capillary action was proposed to express the water movement in an unsaturated wet porous body. This equation was applied to the movement of condensed water in micro-capillaries within the hygroscopic porous body and it was found that the Kozeny constant varies inversly as the ratio of the amount of capillary condensed water to the total moisture content: $K_c \propto X^*/X_l$, as is shown in CHAPTER 4. Futhermore in CHAPTER's 5 and 6, this relation was confirmed by comparing the experimental drying data of the activated alumina with calculated value .

The object of this chapter is to confirm whether this simple relation can be applied to movement of liquid water in coarse capillaries ($\cong$ 1 μm) in a non-hygroscopic porous body on drying, and to simulate the drying process using this water movement model and the drying model of nonhygroscopic porous body proposed by Toei [21].

7-2 Experimental Results

The model material employed is an unglazed alumina-based ceramic. The experimental details are described in the previous study [20]. Fig. 7-1 indicates the cumulative pore-volume and surface-area distributions determined by the mercury penetration technique. The pore distributes 0.1 μm ~ 50 μm, and thus this material is relatively macrocapillary-porous in comparison with the materials used up to CHAPTER 6. The moisture content, X, can be calculated by the equation; $X = \rho_l [V_t - V(r)]$, using the cumulative pore-volume distribution $V(r)$in this figure.

Figs. 7-2 and 7-3 illustrate the experimental results. As may be seen from Fig. 7-3, the drying process was isothermal during all the period of drying except t < 2h in this experiment.

The critical moisture content was established during 5h < t_c < 6h and the surface moisture-content at this point X_c was 0.22 (see Fig. 7-2). The value of S_c determined from Fig. 7-2 is 1.09×10^2 $m^2 \cdot kg^{-1}$. The value of X_c is equivalent to the maximum amount of unremovable pendular water, as will be mentioned in Section 7.3.

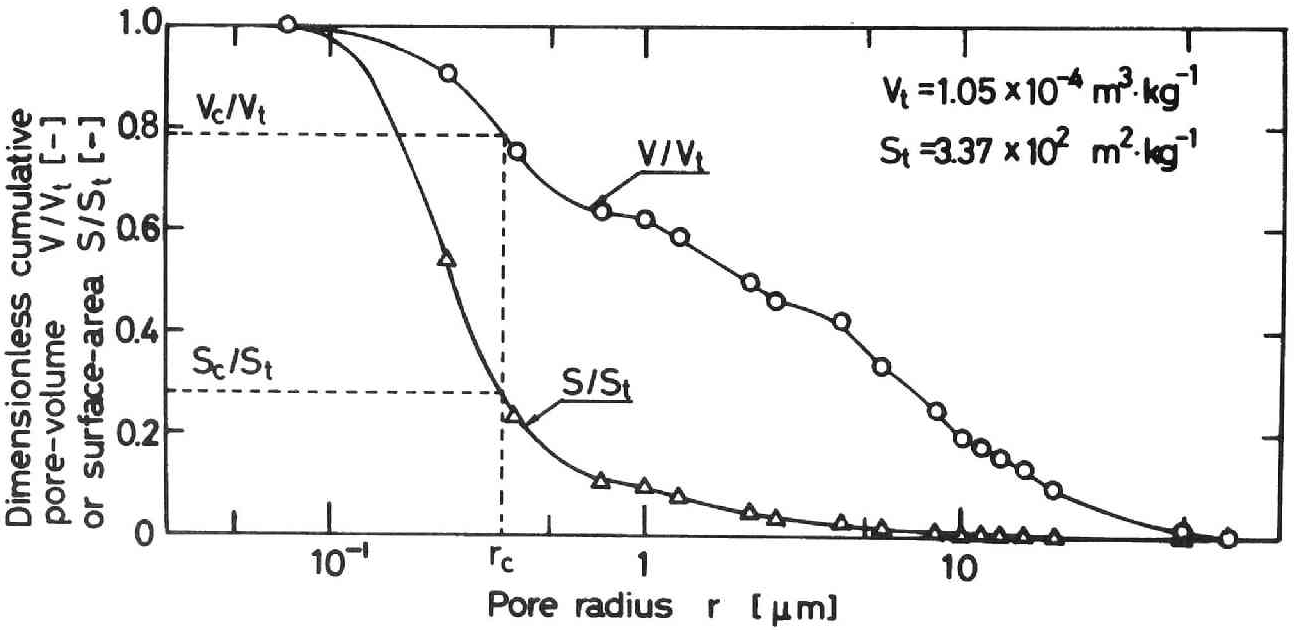

Fig. 7-1. Cumulative pore-volume and surface-area distributions.
(unglazed alumina-based ceramic)

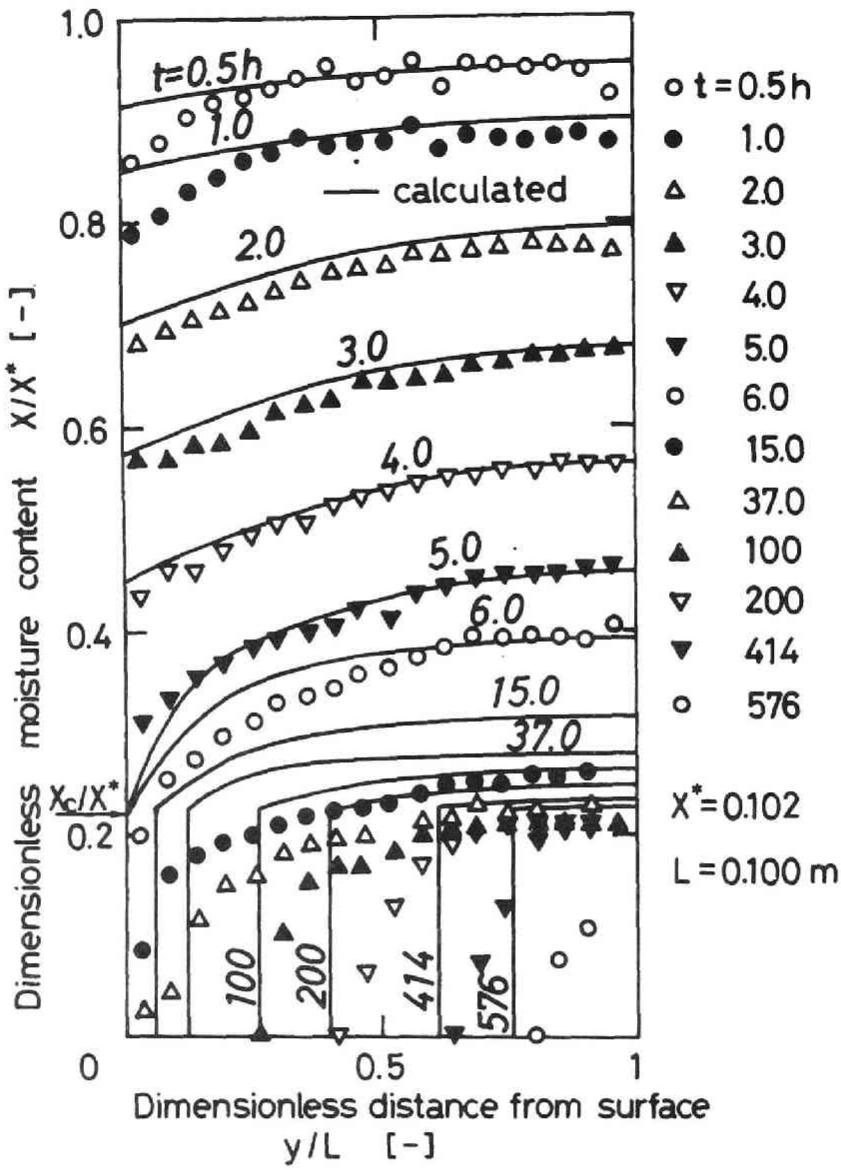

Fig. 7-2. Moisture-content profiles.

(unglazed alumina-based ceramic, 38 °C)

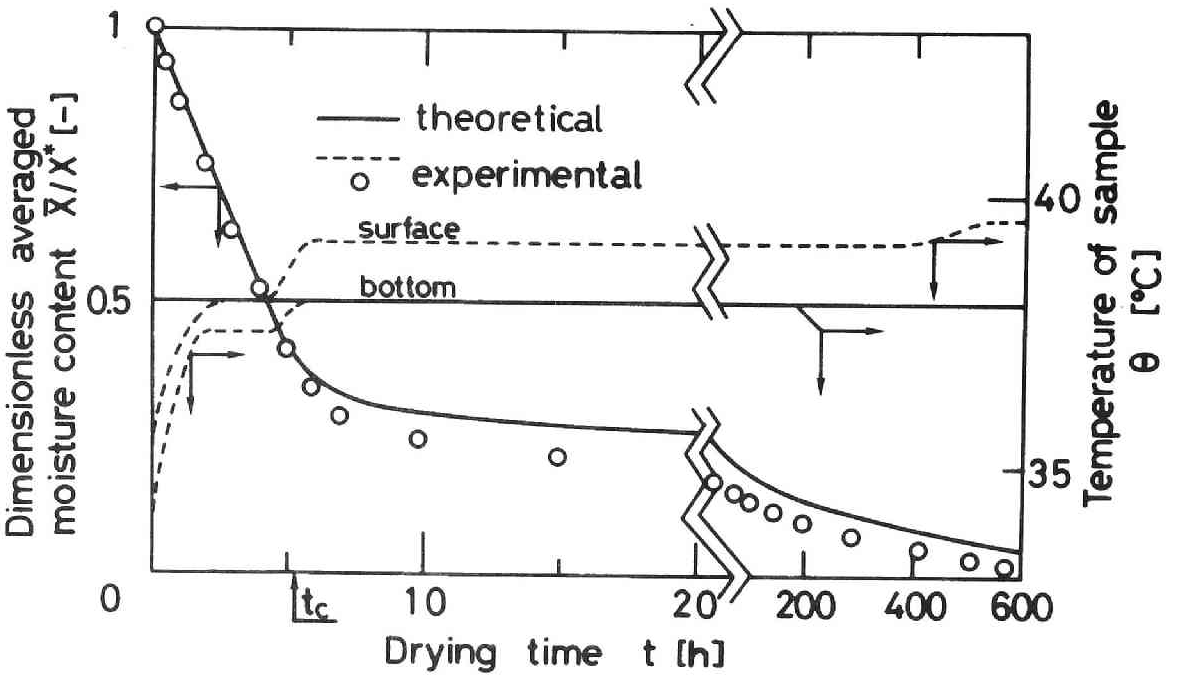

Fig. 7-3. Drying curve and temperature change of sample with time.
(unglazed alumina-based ceramic, 38 °C)

7.3 Theory

It was found that the liquid water in the non-hygroscopic capillary porous body is classified into two groups [18]: funicular water capable of flowing in liquid state ($X_c < X \leqq X^*$), and pendular water that evaporates on the spot and moves in vapor state ($0 < X \leqq X_c$). In accordance with this fact a mathematical model capable of describing the drying process of non-hygroscopic material was proposed by Toei [21]. Since the experimental drying process is regarded as the isothermal one, the following mathematical expressions are derived under an isothermal condition. The mathematical analysis of the drying problem is divided into the constant-rate and the receding-front (falling-rate) periods.

During the period of constant drying rate the capillary potential causes almost all the liquid water to move toward the surface, where it evaporates, and the vapor transfer within the body can be ignored. If the liquid flow of the funicular water in the body due to a gradient in the capillary pressure is expressed in terms of the modified Kozeny-Carman equation derived for the condensed water in the hygroscopic microcapillary-porous body in Section 2.4, the flux is given by *

---

* The water held within the hygroscopic microcapillary porous body is classified into the adsorption water and the capillary condensed water. The modified Kozeny-Carman equation was applied to the whole capillary condensed water and the relation $K_c \propto X^*/X_l$ was found.

In the case of non-hygroscopic macrocapillary porous body, however, as there exists no adsorption water, all the water held in the body is regarded as the capillary water and it is assumed that the modified equation is applied only to the funicular water instead of the whole capillary condensed water. Consequently the relation is written as $K_c \propto (X^* - X_c)/(X - X_c)$.

Futhermore, as the vapor pressure depression in accordance with the Kelvin equation is caused in the fine capillaries, the capillary pressure and the vapor pressure are combined together by Eqs. (2-2) and (2-28).

$$J_l = -\rho_{sapp} D_l \frac{dX}{dy}$$

$$= -\rho_{sapp} D_{l0} \left(\frac{T}{T_0}\right) \left(\frac{\mu_{l0}}{\mu_l}\right) \left(\frac{S_c}{S_c - S}\right)^2 \left(\frac{X - X_c}{X^* - X_c}\right)^4 (1/p_v) \frac{dp_v}{dX} \frac{dX}{dy} \quad (7\text{-}1)$$

The constant D_{l0} of Eq. (7-1) can be estimated by use of the reference value of condensed water transfer coefficient at the known value of moisture content at a selected temperature of T_0. Fig 7-4 illustrates the relationship between the value of experimental D_l calculated from the experimental data of the moisture content distribution as a function of time [20] and the curve of theoretical D_l predicted by use of the value of experimental D_l at X/X^* = 0.5 as a reference value. As may be seen from the figure, the predicted curve agrees with the value from the experiment.

The constant-rate period continues till the value of surface moisture content becomes X_c, the drying process in this period can be written mathematically as

$$\frac{\partial X}{\partial t} = \frac{\partial}{\partial y} \left(D_l \frac{\partial X}{\partial y}\right) \quad (7\text{-}2)$$

I. C. $X = X^* \; ; \; 0 \leq y \leq L \; ; \quad t = 0 \quad (7\text{-}3)$

B. C.

$$\frac{\partial}{\partial t} \int_0^L \rho_{sapp} X dy = kg(p_v|_0 - p_{va}) \; ; \; 0 < t \leq t_c \quad (7\text{-}4)$$

$$D_l \frac{\partial X}{\partial y} = 0 \; ; \; y = L \; ; 0 < t \leq t_c \quad (7\text{-}5)$$

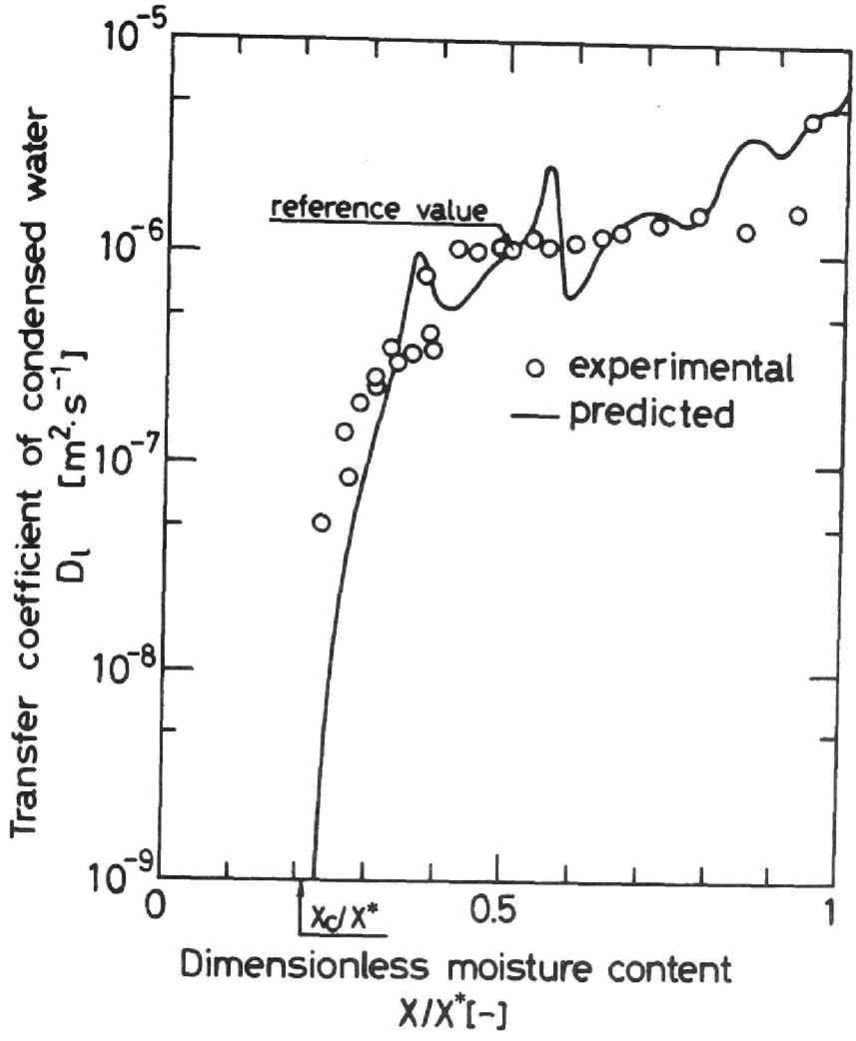

Fig. 7-4. Transfer coefficient of condensed water.
(unglazed alumina-based ceramic, 38 °C)

where $p_v|_0$ can be regarded as the saturation value of p_v at the temperature as is mentioned later.

The surface moisture content falls to zero as soon as it reaches X_c by Toei's model, and this point is the beginning of the receding-front period. In this period the solid is divided into two zones: a dry zone ($0 \leq y < \delta(t)$) and a wet zone ($\delta(t) \leq y \leq L$). The mechanism of the water movement in the wet zone is the same as that in the constant-rate period, and so the water-vapor transfer can be ignored in this zone. Since the moisture content in the dry zone is zero, the water-vapor transfer rate is given by Eq. (7-6) from Eq. (2-13).

$$J_v = - \frac{M_v D_{Kve}}{RT} \left[1 + \left(\frac{p_v}{D_{Kve}} + \frac{p_t - p_v}{D_{Kae}} \right) \frac{B_0}{\mu_{mix}} \right] \frac{dp_t}{dy} \tag{7-6}$$

If a quasi-stationary approximation for the water-vapor transfer is introduced, Eq. (7-6) can be written as the following integrated form.

$$- J_v \delta = \int_{p_t|_0}^{p_t|_\delta} \frac{M_v D_{Kve}}{RT} \left[1 + \left(\frac{p_v}{D_{Kve}} + \frac{p_t - p_v}{D_{Kae}} \right) \frac{B_0}{\mu_{mix}} \right] dp_t$$

$$= \int_{p_t|_0}^{p_t|_\delta} \eta(p_v, p_t)\, dp_t \tag{7-7}$$

where $p_t|_0$ is equivalent to the atmospheric pressure. The

right-hand side of the above equation can be integrated numerically, if the relation between p_v and p_t in this zone is known. This relation can be calculated by solving Eq. (6-5). $(dp_t/dp_v) = f(p_v, p_t)$, numerically for the independent variable, p_v , in the interval of that from $p_v|_0$ to $p_v|_\delta$. The partial vapor pressure at the receding-front, $p_v|_\delta$, is determined from substituting the critical radius, r_c , into the Kelvin equation as a Kelvin radius but this value is almost equivalent to p_v^* , which is the saturated vapor pressure of free water, in the region of the pore radius $r >$ 0.1 μ m. On the other hand, the partial vapor pressure at the drying surface, $p_v|_0$, can be predicted by the following mass-balance equation.

$$k_g(p_v|_0 - p_{va}) = - J_v \qquad (7\text{-}8)$$

where p_{va} means the partial vapor pressure in the drying agent (air). Consequently, the water-vapor transfer rate, J_v, can be determined by Eq. (7-7), (6-5), and (7-8) using a trial and error method. The partial vapor and total pressure profiles can be obtained from the ratio of the integrated form of Eq. (7-6), in the integral interval from $p_t|_0$ to $p_t|_y$ $(0 < y \leq \delta)$, to Eq. (7-7) as is given by Eq. (7-9), because the total-pressure change in the dry zone as the function of the partial vapor pressure can be calculated

by Eq. (6-5).

$$y/\delta = \left[\int_{p_t|_0}^{p_t|_y} \eta(p_v, p_t)\,dp_t\right] \Big/ \left[\int_{p_t|_0}^{p_t|_\delta} \eta(p_v, p_t)\,dp_t\right] \qquad (7\text{-}9)$$

Finally the mathematical expression in this period is

$$\frac{\partial X}{\partial t} = \frac{\partial}{\partial y}\left(D_l \frac{\partial X}{\partial y}\right) \qquad (7\text{-}2)$$

I. C. $X|_0 = X_c \;;\; X = g(y) \;;\; t = t_c$ (7-10)

B. C.

$$\frac{\partial}{\partial t}\int_{\delta(t)}^{L} \rho_{sapp}\, X\, dy = -J_v|_{\delta(t)-} = -J_v;$$

$$X|_{\delta(t)} = X_c \;;\; t > t_c \qquad (7\text{-}11)$$

$$kg(p_v|_0 - p_{va}) = J_v \;;\; t > t_c \qquad (7\text{-}12)$$

$$D_l \frac{\partial X}{\partial y} = 0 \;;\; y = L \;;\; t > t_c \qquad (7\text{-}13)$$

where $X = g(y)$ of Eq. (7-10) is the final moisture profile of the constant-rate period.

7.4 Numerical Results and Discussions

The drying model subject to the boundary conditions given by Eqs. (7-2) - (7-5) and (7-10) - (7-13) were solved by the implicit finite difference technique at 38°C. The calculation method for the constant-rate period is attributed to the problem to find the surface moisture content at $t = t + \Delta t$ by trial and error. It is more complicated to solve in case of the receding-front period,

because more trial-and-error calculations are required to solve Eqs. (7-11) and (7-12) for J_v in the dry zone as is described above in addition to determine the value of δ as a function of t by trial and error. The transport properties obtained from some proper measurement methods and the physical characteristics of the material used to simulate the drying process are given in Table 7-1.

Figs. 7-2 and 7-3 give comparisons of the simulation and experimental results. Agreement between the predicted value and experimental one for the moisture content against time and position during the constant-rate period is satisfactory. This is because the relation $K_c \propto (X^* - X_c)/(X - X_c)$ can be also applied to the non-hygroscopic material. Agreement during the receding-front period, however, is not fairly good. It is believed that the reason for the deviation is ascribed to the assumption that the pendular water never move in liquid state. Fig. 7-2 also gives the positions of receding-front against time. The simulation results are in good agreement with the experimental data. This indicates the diffusion coefficients and the viscous gas flow parameter obtained from entirely independent of any drying experiment can estimate quantitatively the vapor flux in the dry zone.

Table 7-1. Physical characteristics and transport properties for drying of unglazed alumina-based ceramic

ρ_{sapp}	2.79×10^{3}	$kg \cdot m^{-3}$
S_t	3.37×10^{2}	$m^2 \cdot kg^{-1}$
X^*	0.102	(kg-water).kg^{-1}
X_c	2.24×10^{-3}	(kg-water)$\cdot kg^{-1}$
L	0.100	m
k_g	1.55×10^{-7}	(kg-water)$\cdot m^{-2} \cdot s^{-1} \cdot Pa^{-1}$
	determined from the drying rate of constant-rate period.	
p_{va}	7.94×10^{2}	Pa
B_0	5.58×10^{-14}	m^2
	obtained from the permeability measurement using quasi-steady state method.	
D_{Kve}	$3.38 \times 10^{-6}\sqrt{T}$	$m^2 \cdot s^{-1}$
	obtained from the permeability measurement using quasi-steady state method.	
D_{vae}	$1.02 \times 10^{-15} T^{1.75} p_t^{1}$	$m^2 \cdot s^{-1}$
	obtained from the uniform-diffusion measurement. (ε 0.254; q =3.00)	
D_{l0}	1.31×10^{-3}	$m^2 \cdot s^{-1}$
	determined by the reference value of drying experiment at 38 ℃.	

Fig. 7-5 shows the calculation results of the partial vapor and total pressure profiles in the dry zone at 38°C. The maximum generated total-pressure is so small (about 35 Pa) that the treatment of the uniform-pressure diffusion seems to be acceptable in this zone. The water-vapor transfer rate in this case can be written as Eq. (7-14) from Eq. (2-24).

$$J_v(\text{uniform-pressure}) = -\frac{M_v D_{Kve}}{RT} \frac{D_{vae}}{D_{vae} + \frac{p_t - p_v}{p_t} D_{Kve} + \frac{p_v}{p_t} D_{Kae}} \frac{dp_v}{dy} \qquad (7\text{-}14)$$

If the above equation is integrated in the interval of the dry zone, the following equation is given easily.

$$-J_v(\text{uniform-pressure})\,\delta = \frac{M_v p_t D_{vae}}{RT} \ln\left[\frac{1 - \gamma(p_v|_0/p_t) + (D_{vae}/D_{Kve})}{1 - \gamma(p_v|_\delta/p_t) + (D_{vae}/D_{Kve})} \right]$$

$$= \frac{M_v p_t D_{vae}}{RT} \omega(p_v|_\delta) \qquad (7\text{-}15)$$

where

$$\gamma = 1 - \sqrt{M_v/M_a}$$

The partial vapor-pressure profile can be obtained from the ratio of the integrated form in the interval between the drying surface and an arbitrary position within the dry zone to Eq. (7-15), and is written as the following expression similar to Eq. (7-9).

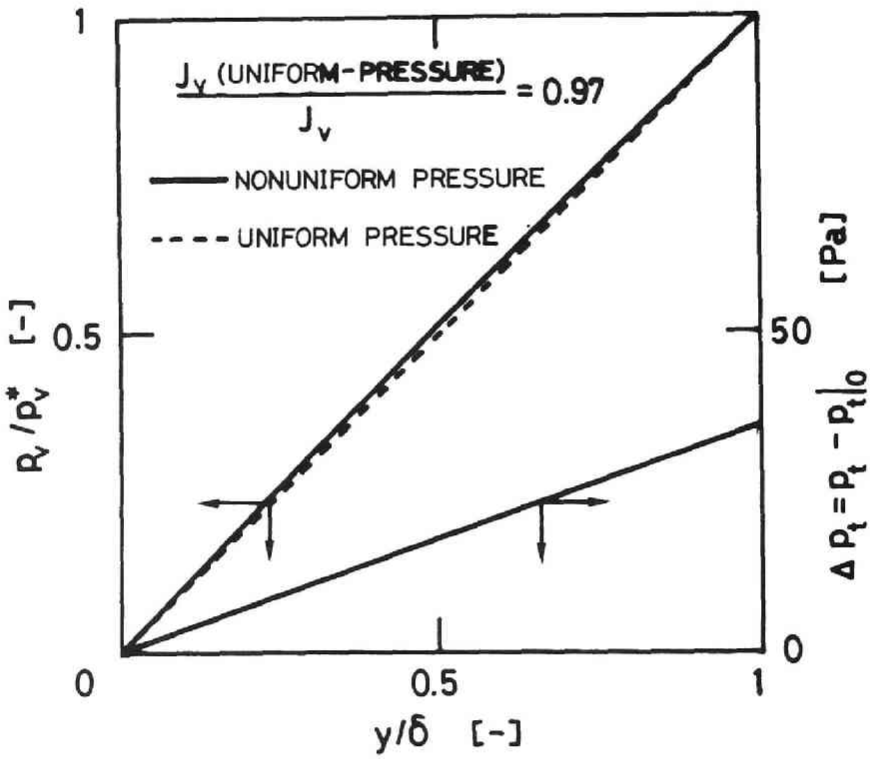

Fig. 7-5. Partial vapor and total pressure profiles in dry zone. (unglazed alumina-based ceramic, 38 ℃)

$$\frac{y}{\delta} = \frac{\omega(p_v|_y)}{\omega(p_v|_\delta)} \qquad (7\text{-}16)$$

The calculated result of the equation, as is shown in Fig. 7-5, agrees well with that of Eq. (7-9). The error of drying rate arising from the assumption of uniform-pressure, which is given as the ratio of Eq. (7-6) to Eq. (7-14), is only three percent.

7-5 Conclusions

The simple relation $K_c \propto X^*/X_l$ in the modified Kozeny-Carman equation capable of describing the movement of the condensed water in the hygroscopic microcapillary-porous material proposed in Section 2.4 is also valid for predicting the transport of the funicular water in the non-hygroscopic macrocapillary-porous body. In this case, however, this relation is rewritten as $K_c \propto (X^* - X_c)/(X - X_c)$.

The simple drying model dividing the drying process into two parts predicts successfully the drying characteristics of the non-hygroscopic capillary-porous body: the drying time for constant-rate period and the position of receding-front as a function of time.

CHAPTER 8 CONCLUSIONS AND FUTURE PROSPECTS

In this thesis, the two kind of hygroscopic microcapillary porous materials (activated alumina) and the non-hygroscopic macrocapillary porous material (unglazed alumina-based ceramic) were used as the experimantal bodies. The transfer rate of capillary condensed water or funicular water within the bodies was estimated by the modified Kozeny-Carman equation, on the basis of the assumption that the Kozeny constant varies inversly as the ratio of the capillary condensed (hygroscopic bodies) or the funicular (non-hygroscopic body) water content to the total moisture content. Since this moisture-content dependent Kozeny variable, however, was not related directly to the pore structure characteristics, the proposed relation of the Kozeny variable is nothing but an experiential one. Despite of this fact, this relation has the important meanings of applications for drying processes on the engineering, because the experimental facts that if the drying material posesses the constant-rate period, the liquid water transfer coefficient is almost constant above the critical moisture content and decreases roughly exponentially with decreasing the moisture content based on the void-volume below the critical one, can be explained by the proposed Kozeny valiable as is shown in Fig. 7-4. Futhermore, this variable

can explain quantitatively the experimental fact that the capillary condensed water transfer coefficient of the hygroscopic microcapillary porous materials decreases roughly exponentially with decreasing the moisture-content ,as is shown in Figs. 4-7 and 6-3, similar to the case of the non-hygroscopic material below the critical moisture content. It seems that the discussions above-mentioned show that the capillary condensed water flow may be related to the pore structure characteristics through the amount of condensed water. To clarify the relation of Kozeny variable between the condensed water content and pore structure characteristics with some proper pore structure model is one of the important subjects on future works.

In order to correlate the parameters defined in Eq. (2-33), which represent the surface flow coefficient, with the pore characteristics, Tamon et al. [17] proposed the following correlating equations for the parameters. These equations give a rough estimation within the error of about ± 50 %.

$$D_{s0} = 3.65 \times 10^{-10} S_t^{0.65} \ m^2.s^{-1}$$

$$a = 0.49$$

In CHAPTER's 4 and 6, the following two sets of parameters were determined for the two kind of activated alumina; the activated alumina used in CHAPTER 4 gives

$$D_{s0}(\text{exp.}) = 6.33 \times 10^{-7}\ m^2 \cdot s^{-1}$$
$$a\ (\text{exp.}) = 0.528$$

and the activated alumina used in CHAPTER 6 gives

$$D_{s0}(\text{exp.}) = 1.78 \times 10^{-5}\ m^2 \cdot s^{-1}$$
$$a\ (\text{exp.}) = 0.64$$

As the total specific surface areas of the two activated alumina were $1.30 \times 10^5\ m^2 \cdot kg^{-1}$ in CHAPTER 4 and $1.79 \times 10^5\ m^2 \cdot kg^{-1}$ in CHAPTER 6, respectively, the next value is obtained for the parameters from the correlating equations; the activated alumina in CHAPTER 4 gives

$$D_{s0}(\text{cal.}) = 7.7 \times 10^{-7}\ m^2 \cdot s^{-1}$$
$$a\ (\text{cal.}) = 0.49$$

and the activated alumina in CHAPTER 6 gives

$$D_{s0}(\text{cal.}) = 9.5 \times 10^{-7}\ m^2 \cdot s^{-1}$$
$$a\ (\text{cal.}) = 0.49$$

The correlating equations give a reasonable result for the activated alumina used in CHAPTER 4, although Eq. (2-33) was derived on the assumption of energical homogeneity of solid surface. The correlating result for the activated alumina in CHAPTER 6, however, is less satisfactory. It seems that the reason for the deviation come out from the insufficiency

of the data in the adsorptin region, because if the value of a is set 0.49, the value of D_{s0} becomes about 10^{-6} $m^2 \cdot s^{-1}$ with less fitting accuracy.

Futhermore, it is necessary to modify the gas-phase transport equations. In the proposed model, the water-vapor flux within the unsaturated wet porous body was assumed to be equal to the flux within the dried up porous body multiplied by the gas void fraction, $(1 - X/X^*)$ but this approximation is nothing but one of rough approximations. In general, whenever the vapor flux has a predominant part of the total flux, the moisture content is lower or zero on almost all drying processes. The assumption, therefore, did not cause fatal errors of simulation results to the experimental data.

If the proposed model or the model modified according to the above-mentioned problems is extended to a non-isothermal system, it is necessary to analyse sufficiently the surface flow phenomenon under the non-isothermal condition, and the statistical thermodynamics will be useful to clarify the phenomenon [15].

The author believes that a mathematical model capable of describing drying processes can be proposed, after these theoretical and experimental difficulties are overcome.

REFERENCES

1. Asaeda, M., M. Okazaki and R. Toei: J. Chem. Eng. Japan, vol.7, 173 (1974).

2. Berger, D. and Pei D.C.T.: Int. J. Heat Mass Transfer, vol.16, 293 (1973).

3. Choong, E.T.: For. Prod. J., vol.13, 489 (1963).

4. Crank, J.: "The mathematics of Diffusion", p.56, 2nd ed., Clarendon Press, Oxford (1975).

5. Dollimore, D. and G.R. Heal: J. Appl. Chem., vol.14, 109 (1964).

6. Fulford, G.D.: Can. J. Chem. Eng., vol.47, 378 (1969).

7. Fuller, E.N., K. Ensley and J.C. Giddings: Ind. Eng. Chem., vol.58, 19 (1966).

8. Horiguchi, Y., R.R. Hudgins and P.L. Silveston: Can. J. Chem. Eng., vol.49, 76 (1971).

9. Kobari, M., Y. Shimizu, M. End and H. Inazumi: Kagaku Kogaku Ronbunshu, vol.8, 521 (1982).

10. Krischer, O.: "Die wissenschaftlichen Grundlagen der Trocknungstechnik", 2nd ed., Springer, Berlin (1963).

11. Luikov, A.V.: "Heat and Mass Transfer in Capillary-porous Bodies", Pergamon, Oxford (1966).

12. Mason, E.A., A.P. Malinauskas and R.B. Evans III: J. Chem. Phys., vol.46, 3199 (1967).

13. Neimark, A.V., L.I. Kheifez and V.B. Fenelonov: Ind. Eng. Chem. Prod. Res. Dev., vol.20, 439 (1981).

14. Novak, L.T. and G.A. Coulman: Can. J. Chem. Eng., vol.53, 60 (1975).

15. Steele, W.A.: "The interaction of Gases with Solid Surfaces", Pergamon, Oxford (1974).

16. Tamon, H., M. Okazaki and R. Toei: AIChE J., vol.27, 271 (1981).

17. Tamon, H., M. Okazaki and R. Toei: AIChE J., to be published in 1985.

18. Toei, R., S. Hayashi, S. Sawada and T. Fujitani: Kagaku Kogaku, vol.29, 525 (1965).

19. Toei, R.: "Shoron Kagaku Kogaku II", Asakura, Tokyo (1967).

20. Toei, R. and M. Okazaki: J. Eng. Phys., vol.19, 464 (Russian) (1970). [English edition: vol.19, 1123 (1970)]

21. Toei, R.: "Advances in Drying vol.2", p.269, Hemisphere, New York (1973).

22. Van Arsdel, W.B.: "Food Dehydration-Principles", vol.1, Avi, Westport (1963).

POSTSCRIPT

This thesis is a collection of some works for drying of porous bodies which were performed by the author in 1979 to 1984 at the laboratory of Professor Ryozo Toei of Kyoto University.

This work covers only a small part of the study on drying mechanism of porous bodies, and many important problems unsolved have been left.

The autor desires that the further studies will be performed and that the final purpose will be accomplished in the near future.